Spin flips – II. Evolution of dark matter halo spin orientation, and its correlation with major mergers

Philip E. Bett[1]⋆† and Carlos S. Frenk[2]

[1]*Argelander-Institut für Astronomie, Universität Bonn, Auf dem Hügel 71, D-53121 Bonn, Germany*
[2]*Institute for Computational Cosmology, University of Durham, South Road, Durham, DH1 3LE, UK*

ABSTRACT

We expand our previous study on the relationship between changes in the orientation of the angular momentum vector of dark matter haloes ('spin flips') and changes in their mass, to cover the full range of halo masses in a simulation cube of length $100 \, h^{-1}$ Mpc. Since strong disturbances to a halo (such as might be indicated by a large change in the spin direction) are likely also to disturb the galaxy evolving within, spin flips could be a mechanism for galaxy morphological transformation without involving major mergers. We find that 35 per cent of haloes have, at some point in their lifetimes, had a spin flip of at least 45° that does not coincide with a major merger. Over 75 per cent of large spin flips coincide with non-major mergers; only a quarter coincide with major mergers. We find a similar picture for changes to the inner halo spin orientation, although here there is an increased likelihood of a flip occurring. Changes in halo angular momentum orientation, and other such measures of halo perturbation, are therefore very important quantities to consider, in addition to halo mergers, when modelling the formation and evolution of galaxies and confronting such models with observations.

Key words: galaxies: evolution – galaxies: haloes – dark matter.

1 INTRODUCTION

One of the key quantities in the evolution of cosmic structures and the formation of galaxies is angular momentum. The acquisition and early growth of angular momentum by dynamically relaxed, overdense clumps of matter ('haloes') can be studied using linear tidal torque theory (Hoyle 1951; Peebles 1969; Doroshkevich 1970a,b; White 1984; Catelan & Theuns 1996a,b; see also Porciani, Dekel & Hoffman 2002; Schäfer 2009; Codis, Pichon & Pogosyan 2015), but this begins to break down as structure growth becomes non-linear (White 1984). Subsequent growth then has to be studied using *N*-body simulations. While research in this field dates back many decades, the continual increase in computing power means that recent simulations have been able to determine with great accuracy the distribution and evolution of the halo angular momentum amplitudes (e.g. Bullock et al. 2001; Avila-Reese et al. 2005; Shaw et al. 2006; Bett et al. 2007, 2010; Hahn et al. 2007a,b; Macciò et al. 2007; Macciò, Dutton & van den Bosch 2008; Knebe & Power 2008; Muñoz-Cuartas et al. 2011).

In contrast, the orientation of halo angular momentum is less well studied. Research on this topic tends to focus on the angular momentum direction with respect to other quantities, such as the shape of the halo (e.g. Warren et al. 1992; Bailin & Steinmetz 2005; Allgood et al. 2006; Shaw et al. 2006; Bett et al. 2007, 2010; Hayashi, Navarro & Springel 2007), the orientation of galaxies (e.g. van den Bosch et al. 2002; van den Bosch, Abel & Hernquist 2003; Chen, Jing & Yoshikawa 2003; Gustafsson, Fairbairn & Sommer-Larsen 2006; Croft et al. 2009; Romano-Díaz et al. 2009; Agustsson & Brainerd 2010; Bett et al. 2010; Hahn, Teyssier & Carollo 2010; Deason et al. 2011), or larger scale filaments and voids (e.g. Bailin & Steinmetz 2005; Hahn et al. 2007a,b; Brunino et al. 2007; Cuesta et al. 2008; Paz, Stasyszyn & Padilla 2008; Hahn, Teyssier & Carollo 2010; Libeskind et al. 2012). In particular, Codis et al. (2012) found that low-mass haloes, which have grown through smooth accretion, tend to have their spin vectors aligned parallel to their nearest filament. In contrast, spins in higher mass haloes, which have experienced major mergers, tend to be perpendicular to their filaments.[1] Dubois et al. (2014) showed that this is also true for galaxies. Experiencing more mergers increases the likelihood of perpendicular alignment, whereas a lack of mergers allows a galaxy spin to drift back towards parallel alignment with its filament (Welker et al. 2014).

---

[1] Codis et al. (2012, 2015) refer to the transition between parallel and perpendicular alignment of spin and filament, as a halo grows, as a 'spin flip', determined statistically over a large halo population. Note that, in our paper, we use the term to refer to *any* sudden changes in spin direction in the lifetimes of *individual* haloes.

The evolution of the *Lagrangian* mass comprising $z = 0$ haloes has been studied by Sugerman, Summers & Kamionkowski (2000) and Porciani et al. (2002), who showed that the spin direction changes due to non-linear evolution, with both the average deviation from the initial direction, and the scatter in that angle, increasing with time.

Part of the reason for the importance of angular momentum is the strong link it provides between halo and galaxy evolution. In the standard cosmological model, the matter content of the Universe is dominated by a cold, collisionless component, cold dark matter (CDM). In this paradigm, structures grow hierarchically, through mergers of ever larger objects. Galaxies then form and evolve within these haloes (White & Rees 1978; White & Frenk 1991). The more complex physical processes available to the baryons as they cycle between gas and stars result in galaxy evolution not being strictly hierarchical (e.g. Bower et al. 2006). In models of galaxy formation, the gas is usually assumed to have initially the same angular momentum as the halo, which is then conserved as the gas cools and collapses to form a disc. Thus, the size of the galactic disc is directly related to the dark matter halo's angular momentum (Fall & Efstathiou 1980; Mo, Mao & White 1998; Zavala, Okamoto & Frenk 2008). This idea is widely implemented in semi-analytic models of galaxy formation (White & Frenk 1991, see also the reviews of Baugh 2006 and Benson 2010). It is important to note that this involves only the magnitude of the halo angular momentum, rather than the full vector quantity. It is the vector that is conserved, and standard semi-analytic models at present make no reference to the angular momentum direction.

Morphological changes in galaxies can be brought about through tidal forces (Toomre & Toomre 1972), and indeed a galactic disc can be disrupted completely if the gravitational potential varies strongly enough over a short time-scale. Galaxy formation models thus assume that a sufficiently large galaxy merger event will destroy a disc, randomizing the stellar orbits and forming a spheroid (e.g. Toomre 1977; Barnes 1988, 1992; Barnes & Hernquist 1996; Hernquist 1992, 1993). This has been shown also to occur in numerical simulations of individual mergers (e.g. Naab & Burkert 2003; Bournaud, Jog & Combes 2005; Cox et al. 2006, 2008). However, the details of the merger process, and the properties of the resulting galaxies, depend strongly on the gas richness of the participants (e.g. Stewart et al. 2008, 2009; Hopkins et al. 2009a,b, 2010; Moster et al. 2010), and on the details of the star formation and feedback processes triggered by the merger (e.g. Okamoto et al. 2005; Zavala et al. 2008; Scannapieco et al. 2009).

In Bett & Frenk (2012) (hereafter Paper I), the authors put forward the idea that sudden, large changes in the *direction* of the halo angular momentum vector (hereafter halo *spin* direction, for brevity) are indicative of a significant disturbance to the halo, and that although such changes are usually assumed to only accompany halo mergers, they can also occur without the large mass gain implied by a merger. This would mean that galaxies could be disrupted by processes that are not captured in the galaxy and halo merger trees used in most current modelling, and that sudden changes to the halo angular momentum direction could be a useful proxy to detect such events.

Such events have been seen in *N*-body and hydrodynamical simulations. Okamoto et al. (2005) found that their simulated disc galaxy flipped its orientation (Bett 2010), with subsequent misaligned gas accretion, resulting in a transformation into a bulge, with another disc forming later. Scannapieco et al. (2009) also found that misalignment of a stellar disc with accreting cold gas can result in bulge formation, sometimes destroying the disc, and sometimes

with a new disc forming later. The idealized experiments of Aumer & White (2013) showed clearly the strong and complex impact of gas/halo misalignment on the evolution of the disc and bulge components of a halo's central galaxy. Romano-Díaz et al. (2009) analysed haloes in simulations both with and without baryons, and found that halo spin orientations can change much more drastically than the angular momentum magnitude, and that such large orientation changes are not restricted to major mergers. Welker et al. (2015) also found that it is not just major mergers that can destroy discs, although minor mergers are statistically less likely to do so; the gas content in the galaxies also has an important role.

Following these studies, Padilla et al. (2014) used the distribution of spin flips from haloes in the Millennium II simulation (Boylan-Kolchin et al. 2009) to incorporate their impact stochastically in a semi-analytic galaxy formation model. In their model, flips in galaxy discs act to reduce the disc spin in proportion to the cosine of the orientation change, i.e. larger flips reduce the spin of the disc more. Their model also allows disc instabilities, which cause bursts of star formation, to be triggered by spin flips, rather than by halo mergers explicitly. The authors demonstrate the positive impact that these changes to the model have on the distributions of galaxy properties at different redshifts, such as galaxy luminosity functions, morphological distributions, and star formation rates.

In this paper, we study the relationship between changes in spin orientation and halo merger history, expanding on Paper I. We include haloes of all masses in the *N*-body simulation we use, and pay special attention to those haloes that do not survive to $z = 0$; we also compare our results against the assumptions of mass and angular momentum conservation used in simple halo models. The results emphasize the need for models of galaxy formation to include more information than just the halo mass accretion history when determining galaxy properties, and in particular the transfer of material from disc to spheroidal structures.

In Section 2, we describe the simulation used, the identification and selection of haloes and their merger trees, and the properties on which we focus in our analysis. Section 3 describes our results, both in terms of the distribution of events overall haloes, and during each halo's lifetime, including the impact on inner halo spin directions. We summarize our conclusions in Section 4.

2 SIMULATION DATA AND ANALYSIS

We use the same simulation and methods for analysis as in Paper I. While we describe the important points here, we refer the reader to that paper for further details.

2.1 The hMS simulation, haloes and merger trees

We use a cosmological dark matter *N*-body simulation that has been referred to as hMS,[2] since it was made using the same L-GADGET-2 code and ΛCDM cosmological parameters as the Millennium Simulation (MS; Springel et al. 2005), but with a smaller cube size ($100\,h^{-1}$ Mpc) and higher resolution (900^3 particles of mass $9.518 \times 10^7\,h^{-1}\,M_{\odot}$, and softening $2.4\,h^{-1}$ kpc). The hMS assumes the same cosmological parameters as the MS: writing cosmological density parameters as $\Omega_i(z) = \rho_i(z)/\rho_{\rm crit}(z)$, in terms

---

[2] Other studies using the hMS simulation include Neto et al. (2007), Gao et al. (2008), Boylan-Kolchin et al. (2009), Libeskind et al. (2009), and Bett et al. (2010).

of the mass density[3] of component i and the critical density $\rho_{\rm crit}(z) = 3H(z)^2/(8\pi G)$, where the Hubble parameter is $H(z)$; for the present-day cosmological constant, total mass, and baryonic mass, the hMS uses values of $\Omega_{\Lambda 0} \equiv \Omega_{\Lambda}(z=0) = 0.75$, $\Omega_{\rm M0} = 0.25$, and $\Omega_{\rm b0} = 0.045$, respectively. The present-day value of the Hubble parameter is parametrized in the standard way as $H_0 = 100h$ km s^{-1} Mpc^{-1}, where $h = 0.73$. The spectral index is $n = 1.0$ and the linear-theory mass variance in $8\,h^{-1}$ Mpc spheres at $z = 0$ is given by $\sigma_8 = 0.9$.

We use a halo definition based on linking and separating subhaloes from their associated friends-of-friends (FOF) particle groups according to information in the halo merger trees. The algorithms for both the haloes and merger trees were originally described in Harker et al. (2006), and designed for use with the implementation of the GALFORM semi-analytic galaxy formation model in the MS (Bower et al. 2006).[4] Particle groups are first identified through the (FOF) algorithm (Davis et al. 1985), with a linking length parameter of $b = 0.2$. Self-bound substructures – the main bulk of the halo itself, plus any subhaloes – are then identified using the SUBFIND code (Springel et al. 2001). Each halo-candidate particle group then consists of a main self-bound structure, zero or more self-bound subhaloes, and plus additional particles that are spatially linked through FOF.

The bound substructures can be tracked between the simulation snapshots, identifying progenitors and descendents (see e.g. Paper I; Harker et al. 2006 or Jiang et al. 2014 for details). Using this additional evolution information, the halo catalogue is refined, by separating off subhaloes that are spatially but not dynamically linked to the halo. For example, subhaloes that are just passing through the outskirts of a larger halo are separated. Two haloes joined by a thin bridge of particles (as commonly occurs with FOF) would also be split apart. Bett et al. (2007) compared the spins, shapes, clustering, and visual appearance of these 'merger-tree haloes' against both simple FOF groups and haloes defined using a simple spherical overdensity criterion, and showed that this merger-tree method offers a great improvement in terms of identifying the genuine physical structure of a halo.

The result of the merger tree and halo identification algorithms is a set of haloes (groups of self-bound structures) identified at each snapshot, with at most one descendent and zero or more progenitors. Each halo identified at $z = 0$ is the root of its own tree, which branches into many progenitor haloes at earlier time steps. In this paper, we wish to study how properties of individual haloes evolve. We therefore identify the evolutionary 'track' of a halo, by finding the most massive of its immediate progenitors at each time step. We give an illustration of halo tracks in a merger tree in Fig. 1. The track of the root halo is marked in red: each red halo is the most massive progenitor of its descendent halo. The halo population at a given snapshot is made up of many other haloes than the root halo; however, tracks of other haloes exist that do not survive until $z = 0$. Instead, they merge into a more massive halo at some point. The endpoint of each track in Fig. 1 is highlighted in heavy black lines. Also note that some tracks have no evolution information, since they only exist at one time step before merging into a larger halo.

It is important to note that neither the halo definition nor the merger tree algorithm are by any means unique. The halo merger
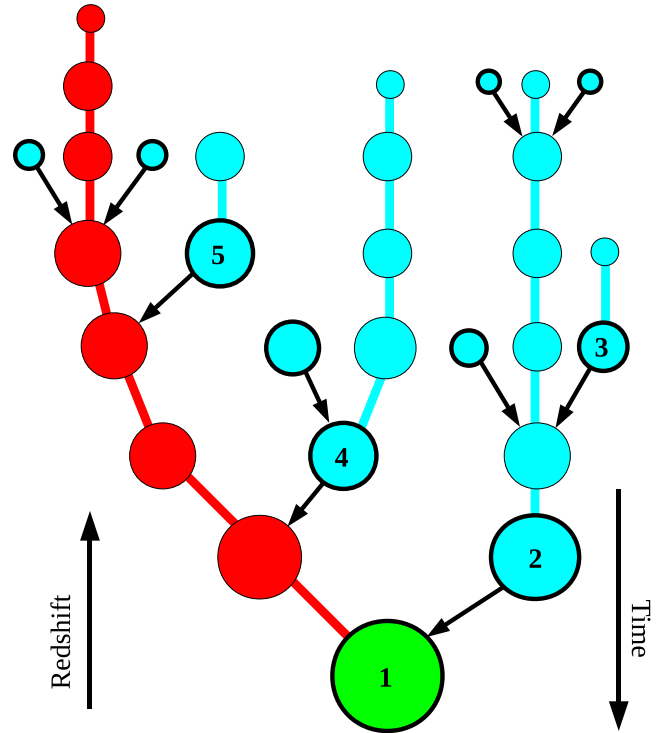
Figure 1. Schematic of a single merger tree. Each circle represents a halo, with each row representing a single simulation output time. The green 'root' halo is that identified at $z = 0$. The evolutionary track of the most-massive progenitors of the root halo is coloured in red. Tracks of haloes that merge into a larger halo before $z = 0$ are coloured cyan. The endpoints of tracks have a heavy black outline, with their final merger into a larger neighbour marked with a black arrow. Six of these 11 tracks only exist at a single time step, leaving five (marked with numbers) with useful halo evolution data.

trees used in the semi-analytic galaxy formation models of Springel et al. (2005) and De Lucia & Blaizot (2007), which also use the MS, construct both the haloes and merger trees differently, although based on similar principles. Other methods that use splitting/stitching algorithms similar to the one used, here, include those by Wechsler et al. (2002), Fakhouri & Ma (2008, 2009), Genel et al. (2009), Neistein, Macciò & Dekel (2010), see also Maller et al. (2006). There have recently been various detailed comparison studies of halo definition and merger tree algorithms, including Tweed et al. (2009), Knebe et al. (2013), Srisawat et al. (2013), and Avila et al. (2014). There is therefore significant scope for similar studies to ours to produce quantitatively different results.

2.2 Halo property catalogues

As in Paper I, various properties of the haloes are computed at each snapshot in time, in the centre-of-momentum frame of each halo, and in physical rather than comoving coordinates. The halo centre is identified with the location of the gravitational potential minimum of its most massive structure, as found by SUBFIND. Properties are computed using the halo particles only (rather than the set of particles within a certain radius), and include the halo mass M, kinetic and potential energies[5] T and U, and angular momentum vector $\boldsymbol{J}$. An approximate 'virial' radius, $R_{\rm vir}$, is found by growing a sphere

---

[3] The equivalent mass–density of the cosmological constant Λ can be written as $\rho_\Lambda = \Lambda c^2/(8\pi G)$.

[4] In particular, they correspond to the DHalo tables in the MS data base (Lemson & the Virgo Consortium 2006).

[5] Following Bett et al. (2007), the potential energy, U, is computed using a random sample of 1000 particles if the halo has more than that.

around the halo centre until the enclosed density from halo particles drops below $\Delta_c(z)\,\rho_{crit}(z)$. The threshold overdensity with respect to critical, $\Delta_c(z)$, is given by the spherical collapse model (Eke, Cole & Frenk 1996), using the fitting formula of Bryan & Norman (1998):

$$\Delta_c(z) = 18\pi^2 + 82\,(\Omega_M(z) - 1) - 39\,(\Omega_M(z) - 1)^2\,. \tag{1}$$

In the case of the flat ΛCDM universe, here, we can write $\Omega_M(z) = \Omega_{M0}a^{-3}/\chi(z)$ and $\rho_{crit}(z) = \rho_{crit,0}\,\chi(z)$, where the expansion factor $a = (1 + z)^{-1}$, and we define $\chi(z) = \Omega_{M0}a^{-3} + \Omega_{\Lambda0}$ for convenience. Note that we only use R_{vir} as a convenient spatial scale for the haloes, rather than as a halo boundary. We also define an inner halo region at $r_{inner} = 0.25R_{vir}$ (following the orientation resolution tests of Bett et al. 2010). Using the mass within this radius, we also compute the inner angular momentum vector $\boldsymbol{J}_{inner}$.

2.3 Halo selection

We need to select haloes at each time step from which reliable measurements of angular momentum can be made. We follow the *Three Rs* of selecting haloes from simulations, requiring them to be well-*r*esolved, approximately *r*elaxed, and *r*obust against effects caused by using discrete particles. These are realized through the following selection criteria, respectively:

$N_p \geq N_{p,lim}$

$|Q| \leq Q_{lim}$,

$\log_{10}\tilde{\jmath} \geq \log_{10}\tilde{\jmath}_{lim}$,

where N_p is the number of particles comprising the halo, the energy ratio $Q = 2T/U + 1$ approximates the virial ratio, and $\tilde{\jmath} = j/\sqrt{GM_hR_{vir}}$ represents a scaling of the halo angular momentum magnitude with respect to that of a particle orbiting under gravity at the virial radius ($j = J/M$ is the specific angular momentum).[6] Following resolution tests in the studies of Bett et al. (2007, 2010), we choose limiting values of $N_{p,lim} = 1000$ (that is, halo masses greater than $\sim 10^{11}\,h^{-1}\,M_\odot$), $Q_{lim} = 0.5$, and $\log_{10}\tilde{\jmath}_{lim} = -1.5$. When considering changes to the inner halo, the criteria for N_p and $\tilde{\jmath}$ are replaced by limits on $N_{p,inner}$ and $\tilde{\jmath}_{inner}$, using the same threshold values.

As in Paper I, we apply two additional selection criteria suggested by a visual inspection of the time series of properties of individual haloes. First, we use a simple measure of 'formation time': we restrict our analysis to the time period after the last time when $M(z) < M_{form}$, and choose $M_{form} = 0.5M_0$ (where M_0 is the halo mass at $z = 0$). Before this time, haloes tend to have a much higher rate of accretion and mergers, and experience a general instability in their properties. Excluding this period ensures that this does not dominate our results. While this undoubtedly affects the number of major mergers that we expect to see in our sample, we are still interested in how spin orientation changes are distributed amongst mass changes large and small; we're not explicitly excluding post-'formation' major mergers.

Secondly, we found that the halo finder and merger tree algorithms sometimes joined a satellite halo into a larger object as a subhalo, and then separated it off again at the next time step, perhaps merging again later. This will clearly cause large apparent changes to the halo angular momentum, mimicking a physical spin

flip; however, it is due to uncertainty in the halo boundary, rather than a physical change in the halo angular momentum. In order to eliminate such 'fake flips', we exclude events with large changes in the virial ratio; in particular, events with $\Delta Q \leq -0.3$ are excluded. Since this effect is due to uncertainties in the halo boundary, we do not apply this exclusion criterion when considering the inner halo spin.

Finally, we note that we analyse our halo population over the redshift range $z < 6.2$; in any case, the effects that we describe will be most observable at low redshift.

2.4 Evolution of halo properties

Combining the merger tree data with the halo catalogues at each time step means, we can obtain the time series of the evolution of each halo property, for each halo (more precisely: for each halo *track*, both those that survive until $z = 0$ and those that do not). As in Paper I, we are most interested in the changes in halo mass and spin orientation over time. We therefore define the same two key quantities used in the previous paper, the fractional mass change,

$$\Delta\mu(t) := \frac{M(t) - M(t - \tau)}{M(t)}, \tag{2}$$

and the change in spin orientation

$$\cos\theta(t) := \frac{\boldsymbol{J}(t)\cdot\boldsymbol{J}(t - \tau)}{|\boldsymbol{J}(t)|\,|\boldsymbol{J}(t - \tau)|}, \tag{3}$$

where τ is the time-scale over which we measure the halo property change (the time $t - \tau$ precedes the time t).

To allow a fair comparison between spin flips in different sizes of haloes at different times, we use a constant time-scale τ, rather than simply using the (irregular) time difference between simulation snapshots. We linearly interpolate halo properties between snapshots to get their values at each 'previous' time $t - \tau$. (The simulation snapshots are sufficiently well spaced in time so that a more complex interpolation scheme is unnecessary.) We choose an event time-scale of $\tau = 0.5\,\mathrm{Gyr}$. The snapshot spacing and the impact of our choice of dynamic time-scale are shown in Appendix A.

We will refer to the halo property changes at a given time step, $\Delta\mu(t)$ and $\cos\theta(t)$, generically as an *event*. We shall use some fiducial values to divide the distribution of events and aid interpretation: we consider a spin direction change of at least $\theta_0 = 45°$ to be 'large', and a fractional mass change of more than $\Delta\mu_0 = 0.3$ to correspond to a major merger. For the sake of brevity, we shall often refer to events with $\Delta\mu \leq 0.3$ as minor mergers, even though they could be smooth accretion (i.e. mass-gain from particles that were not from a separate satellite halo), or even mass-loss. Note that the only restriction on $\Delta\mu$ is that it must be below unity. A value of $\Delta\mu = \frac{1}{3}$ corresponds to a mass-gain of 50 per cent; our fiducial value of $\Delta\mu = 0.3$ results in a slightly smaller gain of $\frac{3}{7} \approx 43$ per cent. If $\Delta\mu > \frac{1}{2}$, then the halo has more than doubled in mass. We expect such events to be rare (but not impossible), due to how the merger trees are constructed: we are always comparing a halo with its most massive progenitor. On the other hand, it is also possible for mass to be lost between time steps, although again our prejudice is for this to be rare. A value of $\Delta\mu = -1$ corresponds to a mass-loss of 50 per cent.

Finally, note that, as we are focusing on events that can disturb a halo, we are not distinguishing between mergers of two similar-mass haloes and the accretion of multiple small haloes on to a larger one: both cases could be registered as 'major mergers' if they

---

[6] Note that $\tilde{\jmath}$ is identical to the alternative spin parameter λ' introduced by Bullock et al. (2001), modulo a factor of $\sqrt{2}$.
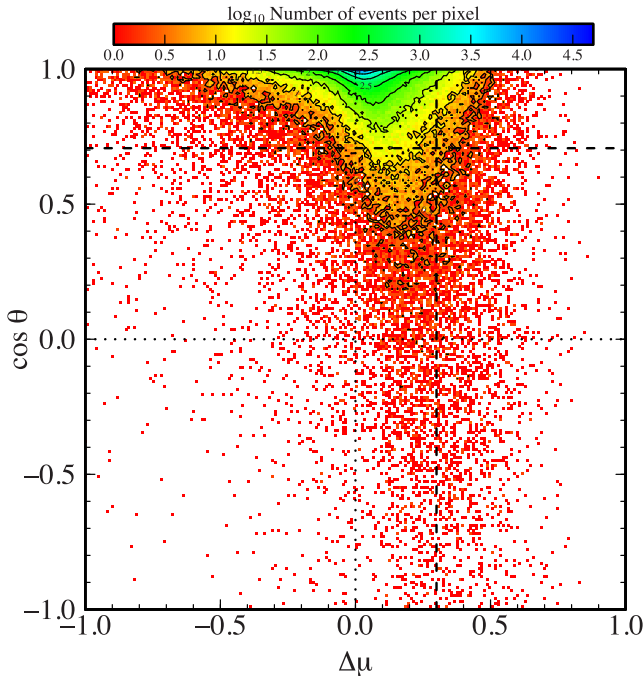
Figure 2. Event distribution in terms of fractional mass change, $\Delta\mu$, and angular momentum orientation change, $\cos\theta$. Dotted lines mark the origin, and dashed lines indicate our fiducial critical values for major mergers ($\Delta\mu > 0.3$) and large flips ($\theta \geq 45°$). Contours are drawn at the levels given by the tickmarks on the colour bar.

occur rapidly enough, such as between two snapshots. Similarly, we do not consider the direction of halo accretion. On the other hand, rapid merging of haloes from opposite directions (e.g. along a filament) is likely to result in rather chaotic changes in spin direction – the infalling haloes would have to have extremely well-balanced angular momenta for them to cancel sufficiently for the direction of the vector to remain unchanged, even if their magnitudes nearly cancelled (although the mass gain would still mean that it would be seen as a 'disruptive' event). The frequency of such events would have to be assessed in simulations with higher time resolution, and we note that our results can, in that sense, be seen as a lower limit: more spin flips might be seen in simulations with more time steps.

3 RESULTS

3.1 Flips of the whole halo

3.1.1 Distribution of flip and merger events

The joint distribution of spin direction changes and fractional mass changes, for all 524 668 selected events from halo tracks after $z = 6.2$, is shown in Fig. 2 (note that the colour scheme is logarithmic). The distribution is very broad, with a strong peak for events with minimal change ($\cos\theta \approx 1$, $\Delta\mu \approx 0$): There are 318 747 events (60.8 per cent) just in the range $-0.05 < \Delta\mu \leq 0.05$ and $\cos\theta \geq 0.95$. The tail down to larger spin orientation changes (lower $\cos\theta$) appears biased towards positive mass change, i.e. mergers. Note, however, that many events have $\Delta\mu < 0$, i.e. mass-*loss* between time steps. Such events can occur for a number of reasons: just 'noise' related to the halo finder and other algorithms, with individual particles being included/excluded from the haloes from one snapshot to the next, and genuine loss from dynamical encounters. While about 23 per cent of events have $\Delta\mu \leq 0$, only 3.7 per cent
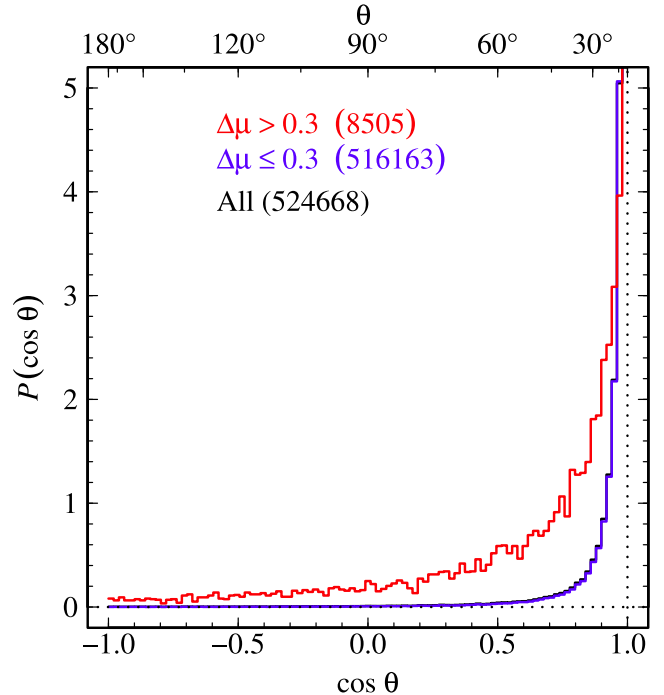
Figure 3. Histograms of $\cos\theta$, cross-sections of the event distribution shown in Fig. 2. The histogram of all events is plotted in black, with the subset corresponding to major mergers in red and minor mergers in blue. Note that the latter lies almost on top of the black line. The number of events selected in each case is written in the legend.

(19 173) have $\Delta\mu \leq -0.1$. Substantial mass-loss is even more rare: just 340 events have $\Delta\mu \leq -1$, which corresponds to a mass-loss of 50 per cent.

To illustrate the shape of the distribution of selected events more quantitatively, we now look at cross-sections through it as histograms. Fig. 3 shows histograms[7] of the spin orientation change for all halo tracks, plus for the subsections of the distribution that correspond to major mergers and minor mergers. The strong spike around 'no change' is clearly visible, but the distribution is significantly broader if only major merger events are considered.
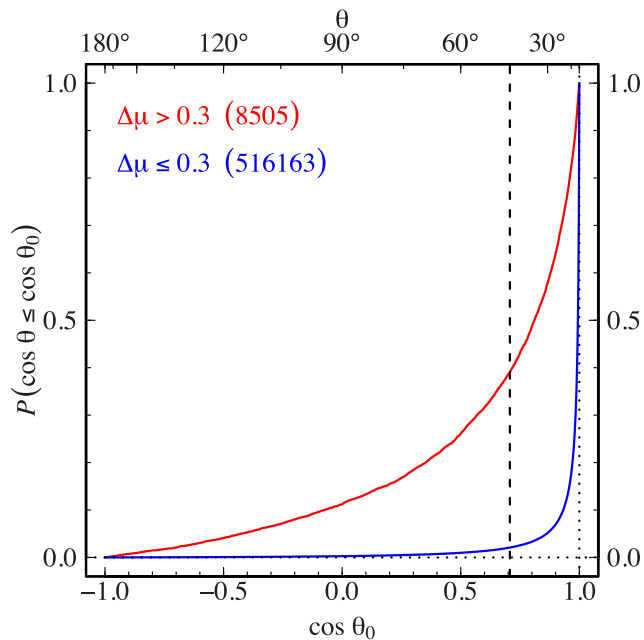
The histogram of halo fractional mass change, for all halo tracks plus the subsets of those that coincide with spin flips of two different magnitudes, is shown in Fig. 4. Again, the spike at 'no change' is clear, but the skewing of the peak of the distribution towards stronger mergers is also visible, particularly, when the histogram is restricted to events with larger spin orientation changes.

The cumulative distribution functions (CDFs) give us additional insight into the relationship between the distributions of spin flips and halo mass changes. We show the CDF of $\cos\theta$ in Fig. 5. This shows that minor mergers are very unlikely to coincide with a large flip: only 2 per cent of events without major mergers had flips of 45° or more. For the major merger events on the other hand, 39 per cent have spin flips of at least that magnitude. However, the CDF of $\Delta\mu$ (Fig. 6) shows that 76 per cent of large flips (45° or more) coincide with *minor* mergers ($\Delta\mu \leq 0.3$). Although these results at first might seem contradictory, they are clearly evident in the shape of the distribution in Fig. 2 and stem from the very large number of minor merger events.

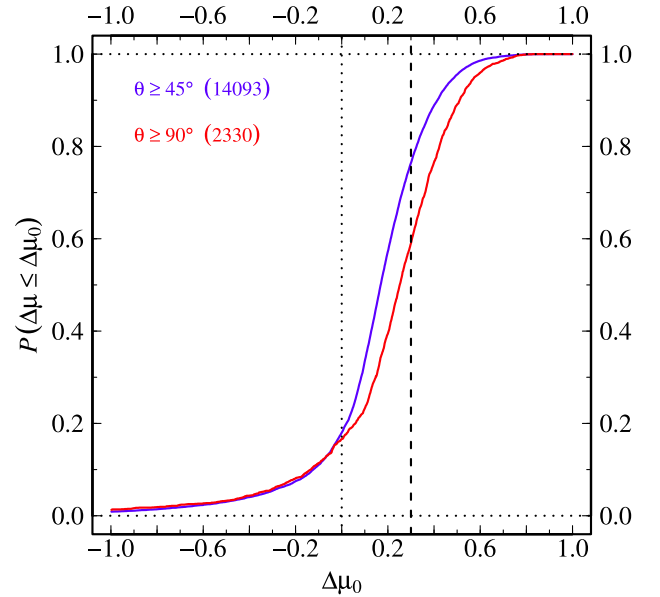[7] Throughout this paper, we show histograms normalized like probability density functions.
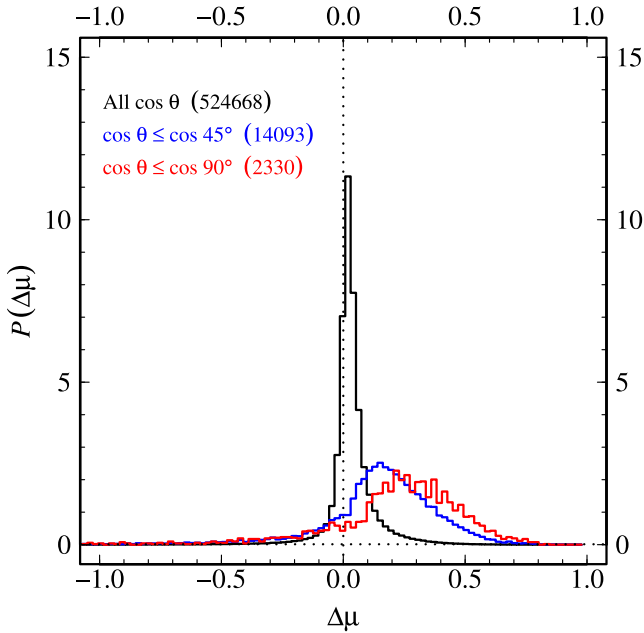
Figure 4. Histograms of $\Delta\mu$, cross-sections of the event distribution shown in Fig. 2. The histogram of all events is shown in black, while that of the subset of events with spin flips of at least $45°$ is shown in blue, and for spin flips of at least $90°$ is shown in red. The number of events selected in each case is written in the legend.

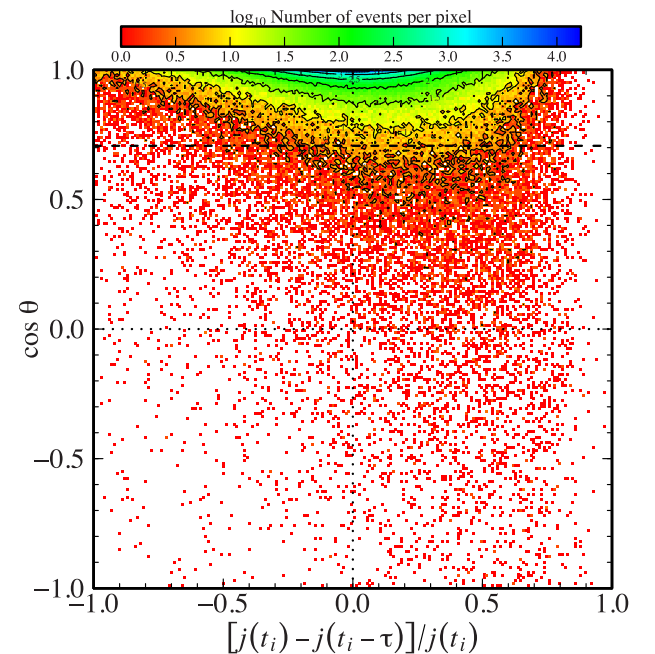**Figure 6.** The cumulative distribution of events with fractional mass change of $\Delta\mu_0$ or less, from the distribution shown in Fig. 2. We show results of selecting just events with spin flips of at least $45°$ (blue) and at least $90°$ (red). Our fiducial value for major mergers, $\Delta\mu > 0.3$, is marked with a dashed line.

Figure 5. The cumulative distribution of events with spin orientation changes of at least θ_0 degrees, from the distribution shown in Fig. 2. We show results of selecting just major merger events ($\Delta\mu > 0.3$, red) and just minor merger events (blue). Our fiducial value of $\theta \geq 45°$ is marked with a dashed line.


Figure 7. Event distribution analogous to Fig. 2, but in terms of the fractional specific angular momentum magnitude change instead of the fractional mass change ($j(t) = J(t)/M(t)$).

There is still a large number of flips in which the spin magnitude does not change, and the spin magnitude can change significantly without a corresponding orientation change.
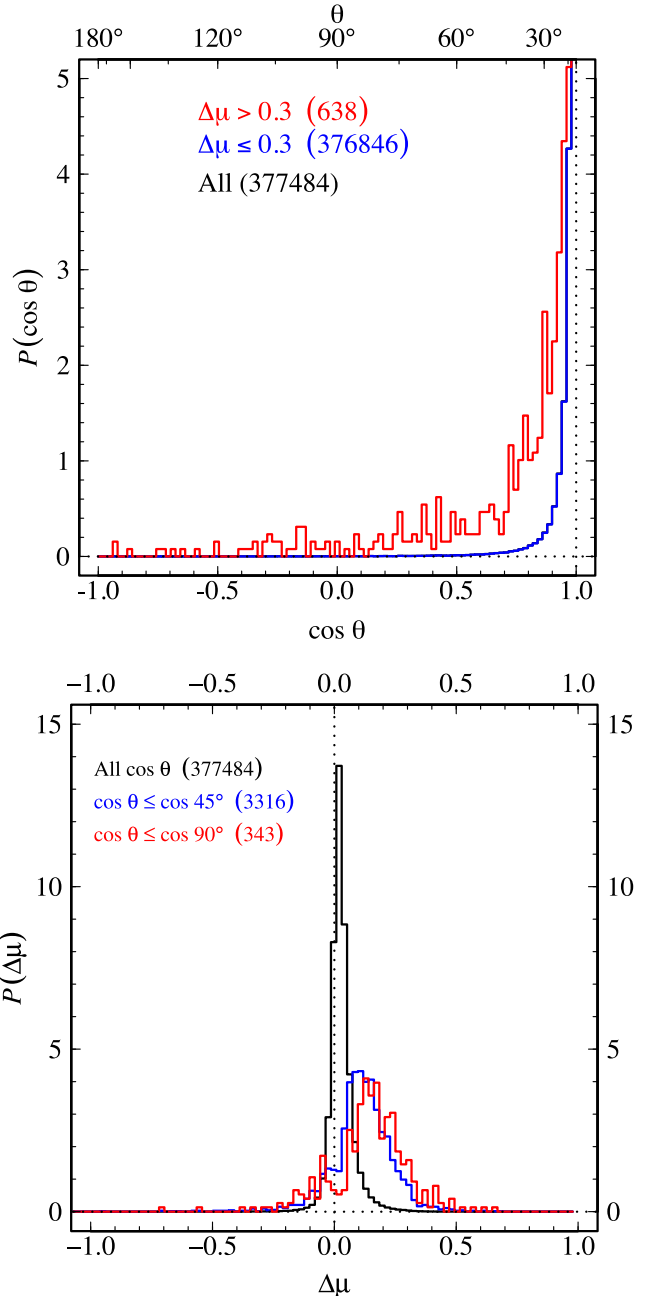
3.1.2 Root tracks versus doomed tracks

We show in Fig. 7 the joint distribution of events in terms of the relative change in halo specific angular momentum *magnitude* versus the orientation change. This serves as an important reminder that a spin flip event does not necessarily mean that the spin magnitude has not also changed. Indeed, there is a weak tendency for large spin flips to correlate with an increase in the halo angular momentum.

We split the event distribution shown in Fig. 2 into that of events in the lives of the root haloes (those still extant at $z = 0$) and
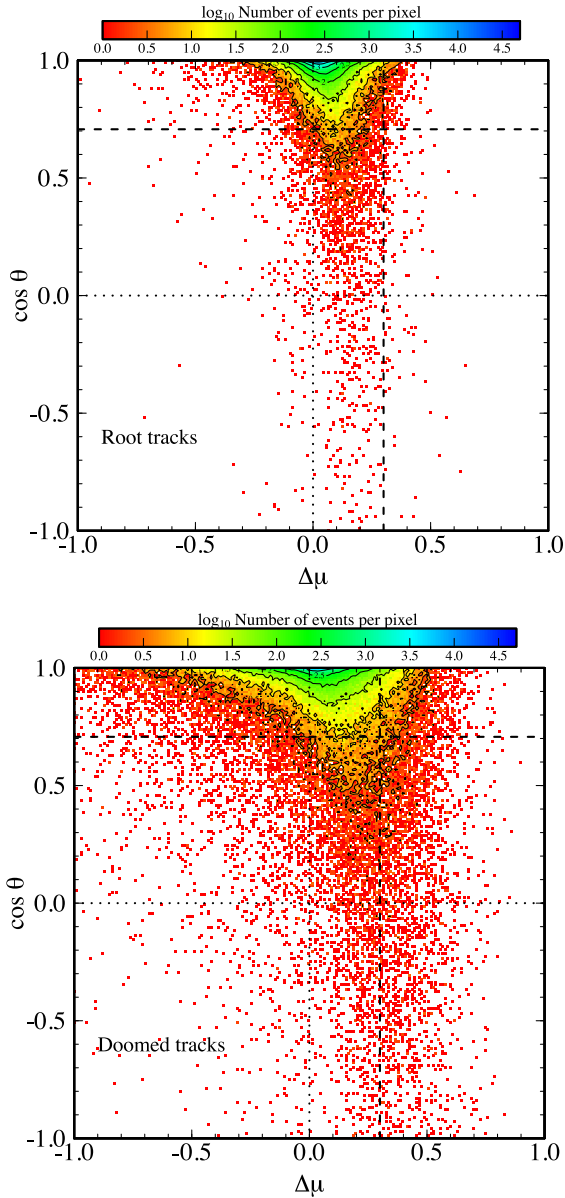
Figure 8. The distribution of events, as in Fig. 2, but split into just the $z = 0$ root tracks only (top) and the doomed tracks only (bottom).

Figure 9. Histograms of the event distribution of root tracks (as shown in the top panel of Fig. 8), in terms of the spin orientation change (top) and the fractional mass change (bottom). These can be compared to Figs 3 and 4.

events in the lives of 'doomed' haloes (those that merge into a more massive halo before $z = 0$). The two resulting event distributions are shown in Fig. 8. Histograms for cross-sections through the root tracks' distribution of 377 484 events are shown in Fig. 9. Although we can see the same basic trends here as in the previous figures (Figs 2–4), the distributions are none the less noticeably different. The root tracks have a much narrower distribution in $\Delta\mu$, visible both at low and high values (mass-loss and major mergers). Much of the broad tail to more negative $\Delta\mu$ seen in Fig. 2 for all tracks seems to come from the doomed tracks.

The cumulative distributions of the events from the root tracks are shown in Fig. 10. When we consider just these haloes that survive to $z = 0$, we find that less than 1 per cent of minor merger events have large spin flips, compared to 23.5 per cent of major mergers. However, over 95 per cent of spin flips of at least $45°$ coincide with minor mergers (88 per cent for flips of at least $90°$).

3.2 The inner angular momentum

To have a noticeable effect on galaxy formation and evolution, it is reasonable to assume that it is the angular momentum in the *inner* regions of the halo in particular that needs to change. We have therefore also looked at the distribution of events from all halo tracks in terms of the angular momentum of the mass located within $0.25R_{\rm vir}$. We show the joint distribution of $\cos\theta_{\rm inner}$ and the total-halo mass change $\Delta\mu$ in the left-hand panel of Fig. 11, with histogram cross-sections of the distribution (as before) in the centre- and right-hand panels. There is an increased likelihood of large spin flips of the inner halo relative to the total-halo results, although the tighter selection criteria (i.e. using $N_{\rm p,inner}$ and $\tilde{\jmath}_{\rm inner}$; see
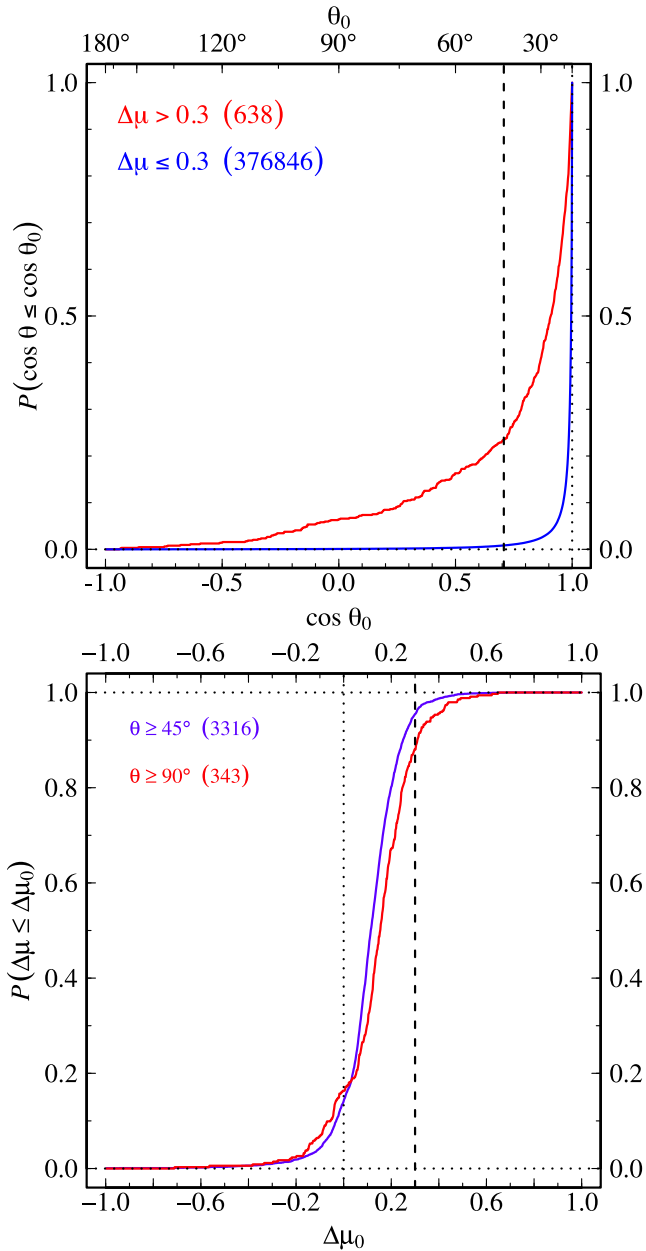
Figure 10. Cumulative distributions of events from haloes on root tracks (as shown in Fig. 8), as a function of flip threshold $\cos \theta_0$ (top) and merger threshold $\Delta \mu_0$ (bottom). These can be compared to Figs 5 and 6.

section 2.3) means there are fewer events selected overall (150 937). This also results in far fewer mass-loss events being selected.

The cumulative distributions for the inner halo spin flip events are shown in Figs 12 and 13. We find that minor merger events (the blue line in Fig. 12) are now much more likely to coincide with a large inner spin flip: about 6.3 per cent, compared to 0.8 per cent for the total-halo flips shown in Fig. 5. The fraction of major merger events that also have significant inner flips is slightly increased, to 43 per cent. When selecting just events with large inner flips (Fig. 13), we find a strong increase in the number that coincides with minor mergers: 95.4 per cent for flips of at least 45° and 91 per cent for flips of at least 90°.

We can also consider the distributions of $\cos \theta_{\text{inner}}$ and $\Delta \mu$ for just the root tracks (Fig. 14). Just as for the total-halo spin, selecting

only the root tracks results in a much narrower distribution of $\Delta \mu$. Although this does not change the cumulative distribution of minor mergers much, there are far fewer large inner flips for the major merger events (compare the middle panel with Fig. 12). The fraction of events with large inner flips that have minor mergers is even higher: over 99 per cent (of the 119 450 selected events) for flips of 45° of more.

3.3 Coincidence of flips and mergers

It would be naïve to assume that, simply because the merger tree algorithm does not register a major merger occurring at exactly the same time as a spin flip, the spin flip is not physically associated with a major merger. For example, a major merger could have occurred at a slightly earlier or slightly later time step in the simulation.

In fact, a visual inspection of the co-evolution of halo properties for individual objects suggests that many large spin flips that appear to coincide with minor mergers actually *do* have a major merger associated with them, albeit at an earlier or later time. For example, the orbit of a satellite halo might take it skimming by the boundary of a halo for a few time steps, affecting the dynamics of the larger halo (causing a flip) before the halo finder deems the satellite to have actually merged. In the case of changes to the inner halo, we might anticipate that the inner spin direction would only change some time *after* a major merger in the halo as a whole, as it might take some time for the dynamics of the inner region to be affected. In this section, we attempt a simple assessment of the importance of such non-coincident flips and mergers, without explicitly considering any causal connections.

For each large flip event ($\theta(t_i) \geq 45°$) from the distribution shown in Fig. 2, we scan the time series of that halo's fractional mass change both before and after the time of the flip, $\Delta \mu(t_i \pm \Delta t)$. We record the time, difference between the flip and the nearest major merger ($\Delta \mu > 0.3$), and plot a histogram of these times, Δt, in Fig. 15. We see that only 45 per cent of these flips (i.e. 6343/14 093) have major mergers that can be identified at *any* time, before or after the flip. For the remaining flip events, no major merger event could be found within the lifetime of the halo. We find that most flips with non-coincident major mergers have the merger preceding the flip, i.e. the angular momentum vector swings round *after* the mass has been incorporated: of the flips with major mergers identified at some point in their lifetimes, there are 2232, with $\Delta t < 0$, versus 790, with $\Delta t > 0$.

The cumulative distribution is shown in Fig. 16. This shows clearly that 23.6 per cent of the large flip events (3320) coincide 'exactly'[8] with major mergers (also seen in Figs 5 and 6). The number of coincident major mergers initially rises very steeply with Δt however. If we allow for major mergers within ± 0.5 Gyr, then the fraction of large flips coinciding with major mergers rises to 33.6 per cent, and then to 38.3 per cent if we extend the window to ± 1 Gyr. Beyond this, the CDF grows slowly, until reaching the maximum at 6343 flips (45 per cent).

We analyse the inner flips in the same way (Figs 17 and 18), based on the event distribution shown in Fig. 11. The histogram shows that, in this case, there are far fewer major mergers following large inner spin flips: 73 per cent (1928) of the inner flips associated with a major merger at any time are preceded by the merger, compared to 250 that are followed by the merger. This is what we would expect: a merger would be initially seen for the halo as a whole, with the inner

---

[8] That is, over the same time steps in the simulation.
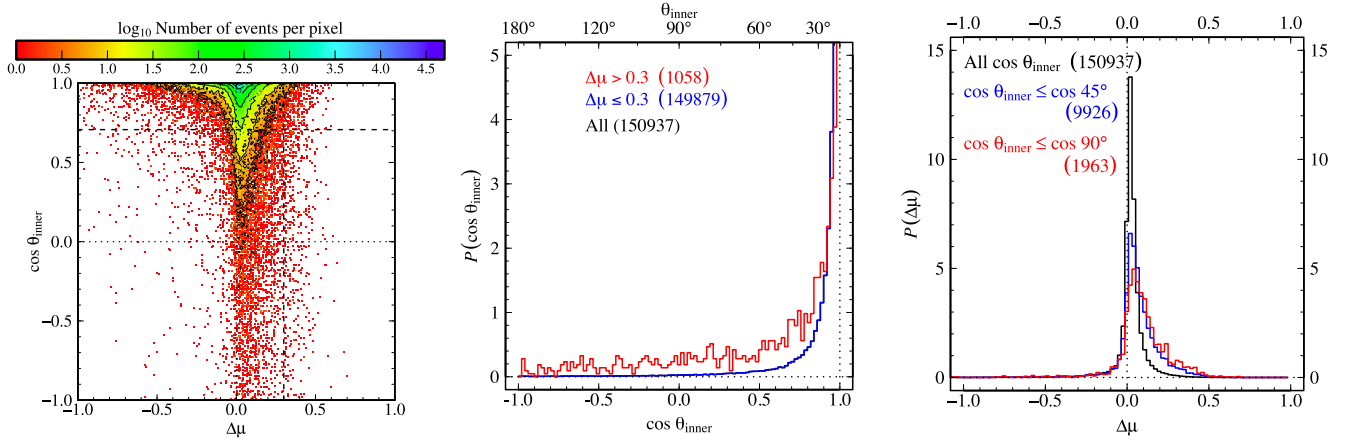
Figure 11. Left: distribution of events from all halo tracks, in terms of the fractional mass change of the total halo, $\Delta\mu$, and the spin orientation change of the inner halo (i.e. the mass within $0.25R_{\rm vir}$). Centre: histogram cross-sections of the event distribution, through $\cos\theta_{\rm inner}$, for all selected events (black) and for the subsets that do (red) and do not (blue) coincide with major mergers. Right: histogram cross-sections through $\Delta\mu$, for all selected events (black) and for those with spin flips of at least $45°$ (blue) and $90°$ (red).
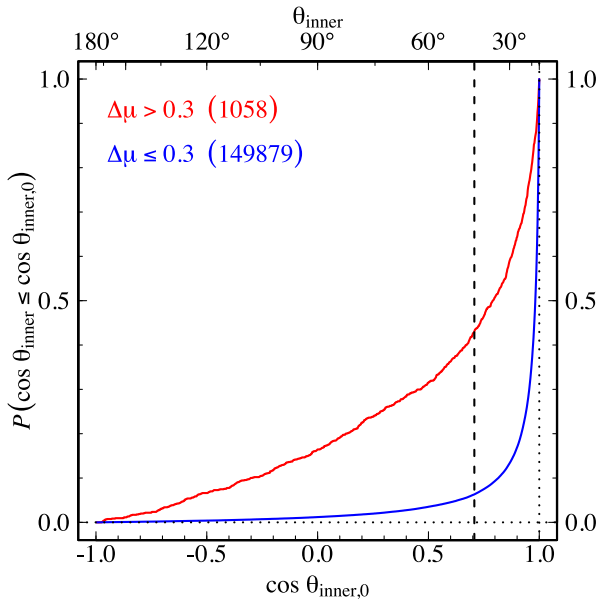
Figure 12. Cumulative distributions of events with inner spin misalignments of at least $\theta_{\rm inner,0}$ degrees. Events are selected as in Fig. 11. We show results taking the limiting total-halo fractional mass change to be $\Delta\mu_0 = 0.3$ (red: major mergers; blue: minor mergers/accretion).
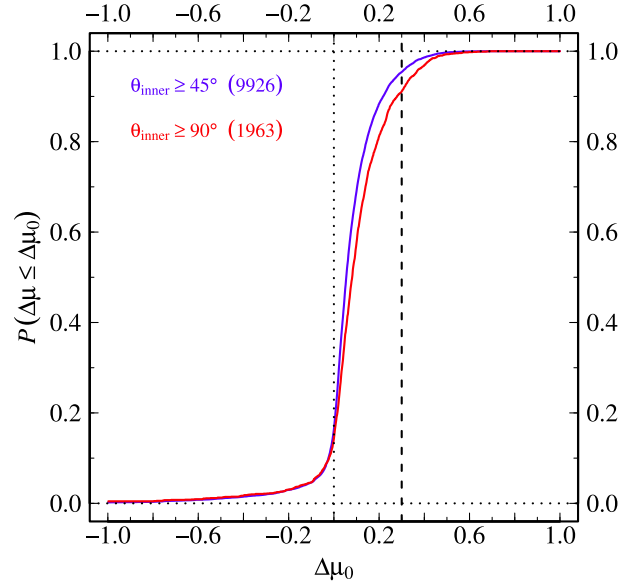
Figure 13. Cumulative distributions of events with fractional mass change of $\Delta\mu_0$ or less, from the event distribution shown in Fig. 11. We show results for selecting just events with inner spin flips of at least $45°$ (blue) and at least $90°$ (red).

halo dynamics reacting a short time later. From the cumulative plot (Fig. 18), we can see that just 26.5 per cent of large inner flips have total-halo major mergers at any time, before or after. As can also be seen in Figs 12 and 13, only 4.6 per cent of flips (455) coincide exactly with a major merger. If we allow for a time lag between a major merger and the inner halo spin direction changing, then we find 10.7 per cent of flips (1065 events) have a merger within $\pm 0.5\,{\rm Gyr}$, rising to 17.6 per cent (1745 events) within $\pm 1\,{\rm Gyr}$.

### 3.4 Spin flips over halo lifetimes

As in Paper I, we now move on to investigate the likelihood of large spin flips occurring over the lifetimes of haloes, rather than the simple distribution of events discussed in the previous sections. We wish to find the probability of a halo undergoing a spin flip of

a given magnitude (θ_0) and duration (τ, the event time-scale), at some point during its lifetime (excluding events at time steps when the angular momentum measurement is not reliable). We can also divide this into spin flips during which the halo's mass does or does not grow by a certain amount, $\Delta\mu_0$ (i.e. considering just flips that do or do not coincide with major mergers).

We show the results for this in Fig. 19. As one might expect, as larger time-scales τ are considered, the likelihood of a halo exhibiting a flip of any given size increases. For our fiducial values of $\theta_0 = 45°$ and $\tau = 0.5\,{\rm Gyr}$, we find that 37.8 per cent of the 40 559 selected haloes exhibit such a flip at some point in their lives. If we consider just those flips that coincide (exactly) with major mergers, this figure is much lower, at 8.3 per cent (see middle panel). Considering just flips that do *not* coincide with major mergers
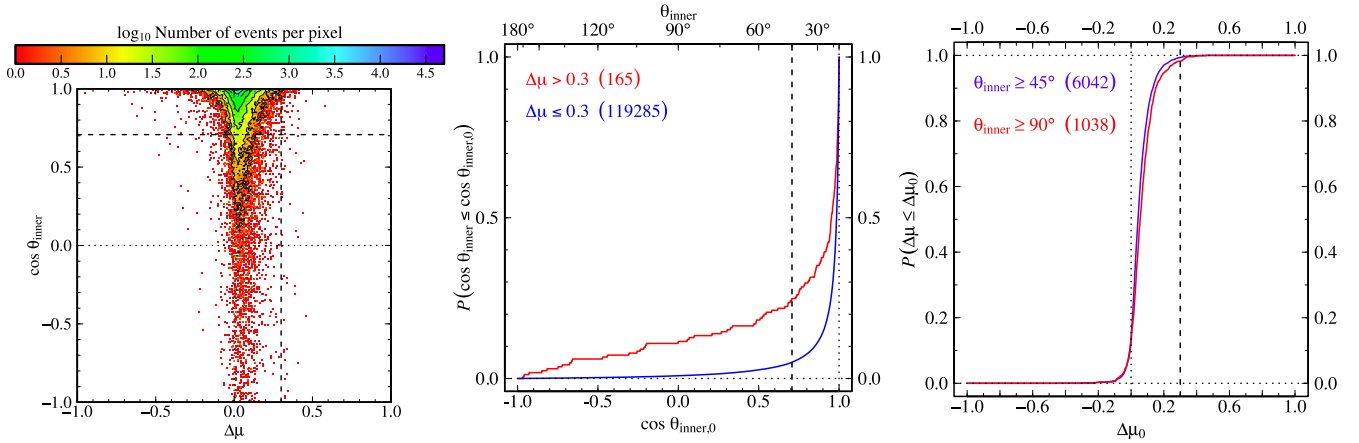
Figure 14. The joint distribution (left) and cumulative distributions (centre, right) of events from root haloes in terms of the total-halo mass change $\Delta\mu$ and inner halo spin orientation change $\cos\theta_{inner}$. These can be compared to Figs 11, 12 and 13.
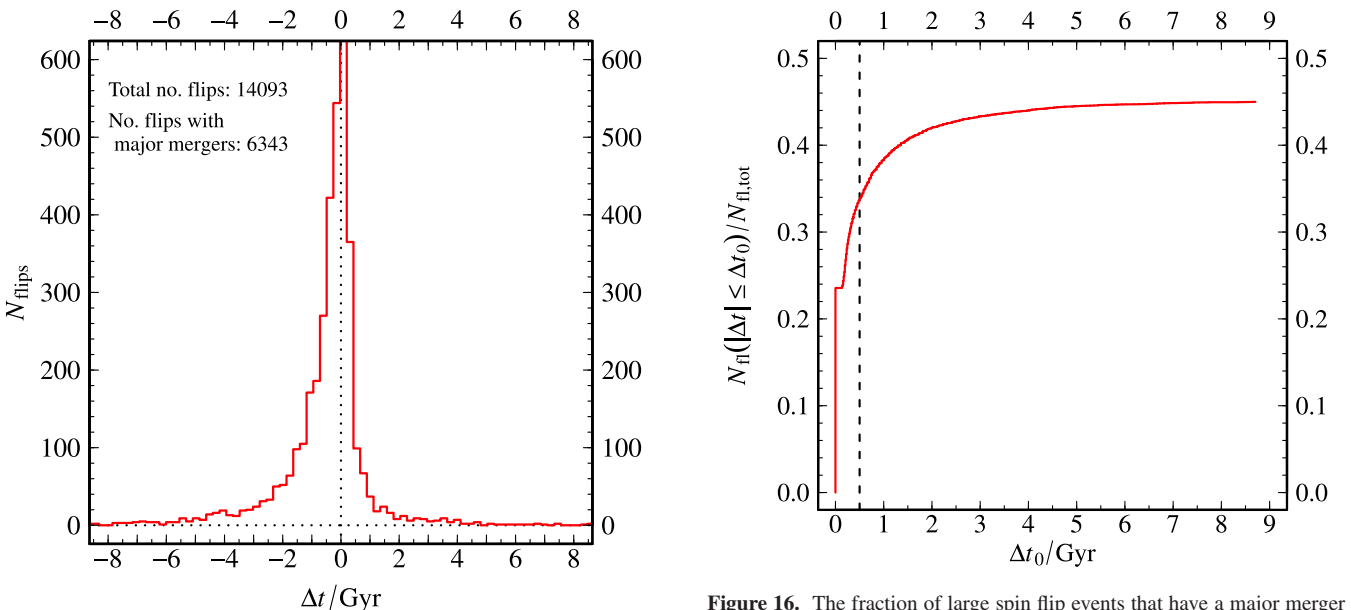
Figure 15. The histogram of the number of spin flip events that have a major merger after ($\Delta t > 0$) or before ($\Delta t < 0$) the flip. The central peak extends to $N_{flips} \sim 3300$.

Figure 16. The fraction of large spin flip events that have a major merger within a time $|\Delta t| \leq \Delta t_0$. Our dynamical time-scale value of $\tau = 0.5$ Gyr is marked with a dashed line.

(right-hand panel), we find that 34.5 per cent of haloes experience such flips.[9]

We perform the same analysis for flips of the inner halo angular momentum in Fig. 20. In this case, haloes are more likely to experience inner spin flips of any magnitude and any duration: 64.1 per cent of the 12 171 selected haloes have inner flips of at least $45°$ over 0.5 Gyr, during the course of their lifetime. As we have seen, fewer inner halo flips coincide with major mergers (e.g. Fig. 18). It is therefore not surprising that, when considering just inner flips that coincide with major mergers, we get a lower fraction of haloes (3.3 per cent) compared to that for the total-halo angular momentum.

Since we have haloes over a wide range of final time masses (both for those that survive to $z = 0$ and the 'doomed' haloes), it is interesting to ask whether there is any mass-dependence in the probability of flips over halo a lifetime. In Fig. 21, we show this in a plot analogous to Fig. 19. In this case, instead of plotting results for different spin flip sizes, we set $\theta_0 = 45°$ and give the results for different bins of final halo mass.

There is a hint of mass-dependence in the probability for flips: lower mass haloes appear slightly more likely to experience a flip of a given time-scale during their lifetime. This trend is reversed when considering flips of the inner halo angular momentum, shown in Fig. 22. In this case, haloes that have larger masses at their final time step are more likely than lower mass haloes to have experienced an inner spin flip at some point in their lifetimes. However, in both the total-halo and inner halo cases, the differences between different mass bins are very slight, and the results from the high-mass bins, in particular, are noisy because they contain relatively few haloes. What trend there is appears stronger when looking at inner flips of

[9] Note that the values for 'All haloes' need not be the sum of those whose flips do and do not coincide with major mergers. A halo can have flips of both kinds during its lifetime, so the categories are not mutually exclusive.
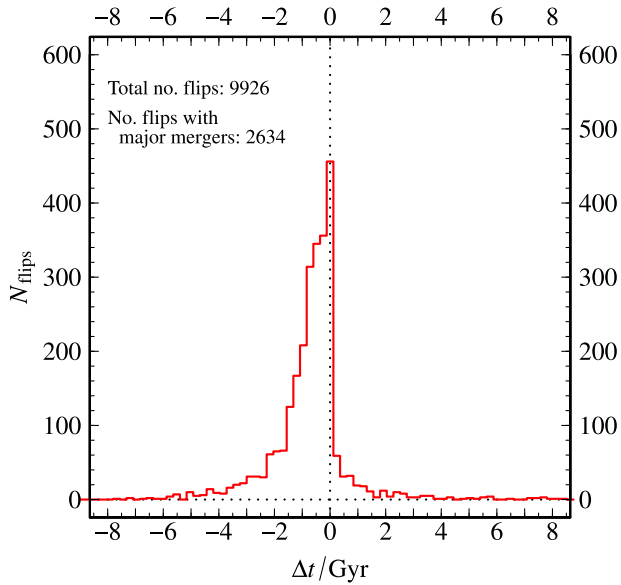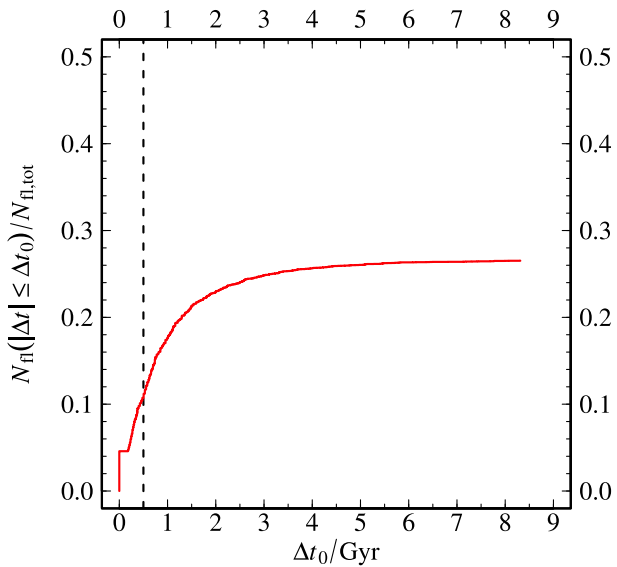
Figure 17. Number of large flips of the inner halo angular momentum that have a (total halo) major merger a certain amount of time, after ($\Delta t > 0$) or before ($\Delta t < 0$) the flip.

Figure 18. The fraction of inner halo flip events that have a total-halo major merger within a time $|\Delta t| \leq \Delta t_0$.

short duration, but is broadly consistent over all values of τ for the total-halo spin flips.

3.5 The contribution of other progenitors

Halo models are commonly used to study the evolution and statistical properties of structures, both in the context of galaxy formation and cosmology in general, such as through Halo Occupation Distribution models (Benson et al. 2000; Berlind & Weinberg 2002) or the Extended Press–Schechter formalism (e.g. Jiang & van den Bosch 2014, and references therein). In such models, the evolution of halo properties such as mass is usually assumed to be solely due to mergers with other haloes. For example, the mass of a halo at one time step is equal to the sum of the masses of its immediate progenitors at the preceding time step. Similarly, since angular momentum

is a conserved quantity, one might assume, in such models, that the halo angular momentum vector is also equal to the sum of the angular momenta of its immediate progenitor haloes. Here, we are able to test the extent to which this assumption holds for the haloes and merger trees we have defined. We illustrate the relationship between immediate progenitors and halo tracks in Fig. 23; in this section, we will be measuring changes in halo properties between a halo at a given time step and the sum of the property over its immediate progenitors. We consider just the root tracks, to avoid double-counting haloes as endpoints of one track and progenitors of another. We also use each simulation snapshot output, rather than interpolating between snapshots to get a constant time-scale τ as in the previous sections.

We compute the fractional mass change between a halo at time, t_i, and the sum of the masses of its N_{prog} immediate progenitors identified at the preceding time step, t_{i-1}:

$$\Delta\mu_{\mathrm{pr}}(t_i) := \frac{M(t_i) - \sum_{p=1}^{N_{\mathrm{prog}}} M_p(t_{i-1})}{M(t_i)}. \tag{4}$$

We can also compute the centre-of-momentum frame for the set of progenitors, and thus, their total angular momentum vector in that frame $\boldsymbol{J}_{\mathrm{progs}} = \sum_{p=1}^{N_{\mathrm{prog}}} \boldsymbol{J}_p$. We can therefore calculate the change in orientation between that total angular momentum of the progenitors and the subsequent halo angular momentum,

$$\cos\phi(t_i) := \frac{\boldsymbol{J}(t_i) \cdot \boldsymbol{J}_{\mathrm{progs}}(t_{i-1})}{|\boldsymbol{J}(t)| \, |\boldsymbol{J}_{\mathrm{progs}}(t_{i-1})|}. \tag{5}$$

In Fig. 24, we plot the joint distribution of events in terms of $\cos\phi$ and $\Delta\mu_{\mathrm{pr}}$ (subject to the same standard selection criteria as before, see section 2.3), along with associated histograms (by analogy to our previous figures).

From these figures, we can see that the assumption that mass is conserved between haloes and their progenitors is quite well founded, i.e. $\Delta\mu_{\mathrm{pr}} \approx 0$. There are relatively few events with large values of $|\Delta\mu_{\mathrm{pr}}|$, with over 84 per cent of the events located within $|\Delta\mu_{\mathrm{pr}}| < 0.05$.

The angular momentum orientation behaves differently. Although it cannot be seen clearly in the joint distribution image (left-hand panel of Fig. 24), the histogram of $\cos\phi$ (middle panel) shows that there is a very strong peak at no change; we find that 40 per cent of the events involve orientation changes of less than 5°. However, there appears to be an almost uniform probability for a change in the orientation of the halo spin with respect to its immediate progenitors, as long as the change is $\phi \gtrsim 45°$. Note that, as mentioned earlier, multiple rapid mergers (between two snapshots) could result in rather chaotic changes in spin direction, as the result depends on the details of the spins and accretion directions of the merging objects. The necessity of using discrete output times means that our results can be seen as a lower limit and could be quantitatively different with different time resolutions.

Thus, while halo mass is reasonably well conserved between time steps, angular momentum is not. This is in agreement with Book et al. (2011), who studied the evolution of angular momentum of individual haloes and their particles in detail.

4 CONCLUSIONS

In this paper, we have investigated the frequency of changes in the spin direction of dark matter haloes over their lifetimes, and how such changes relate to the halo merger history. In a simple
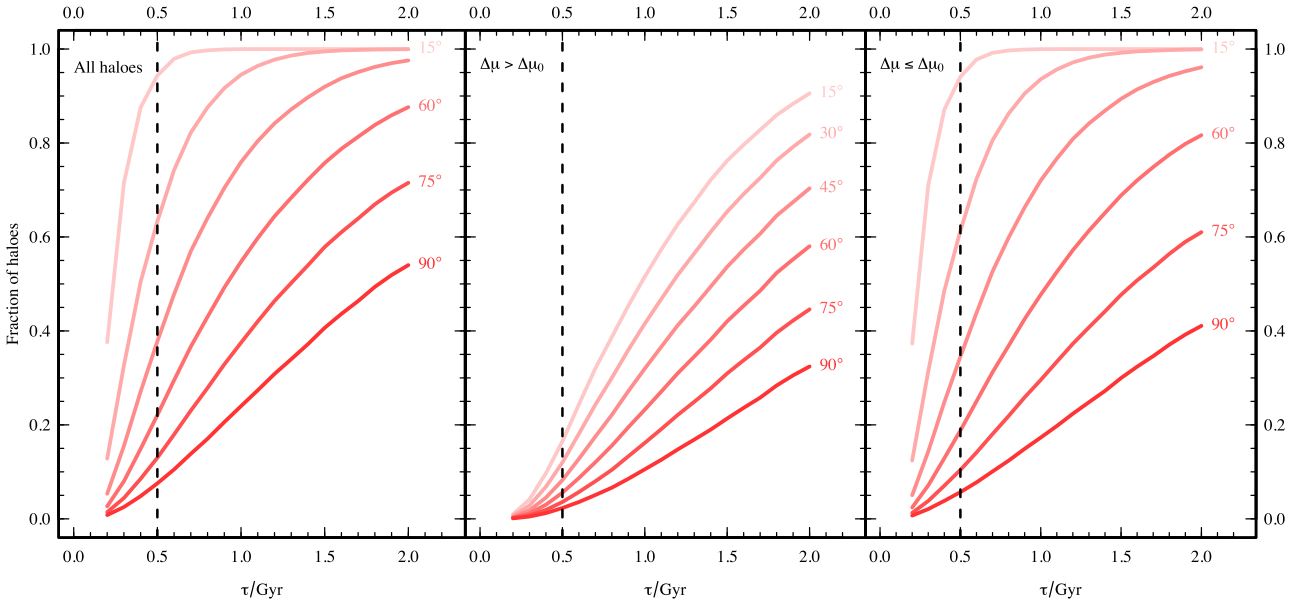
Figure 19. Left: fraction of all halo evolutionary tracks that have at least one spin flip of duration τ and size $\geq \theta_0$. Six values of θ_0 have been chosen, every 15° from 15° to 90°. Middle: fraction of halo tracks with at least one spin flip that coincides with a major merger. Right: same, but for spin flips that do not coincide with a major merger. The characteristic time-scale used in the rest of the paper, $\tau = 0.5\,\text{Gyr}$, is marked with a dashed line.
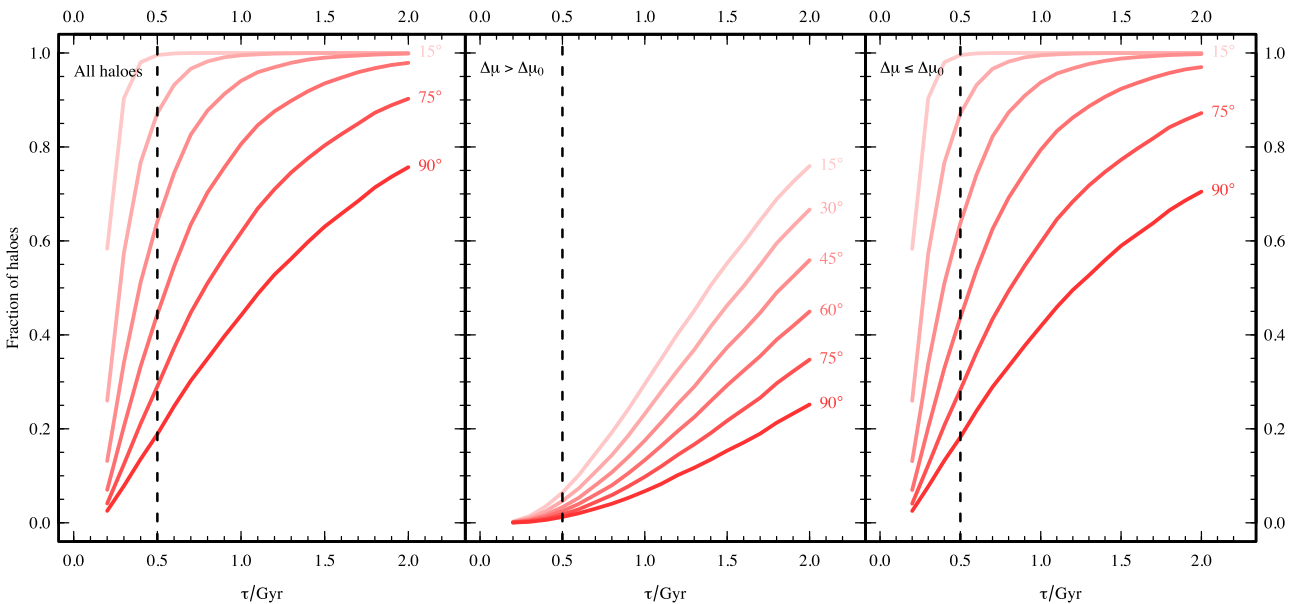
Figure 20. Fraction of all halo tracks that have at least one inner spin flip of at least θ_0 and duration τ (left), and the fractions that have such an inner flip that coincides with a major merger (middle) or does not (right). The same six values of θ_0 are used as in the previous figure. The characteristic time-scale used in the rest of the paper, $\tau = 0.5\,\text{Gyr}$, is marked with a dashed line.

halo model, one might assume that large, sudden changes in spin direction – spin flips – occur exclusively during major mergers, with the angular momentum direction remaining relatively stable during intervening times. Extending the work of Bett & Frenk ([2012](#)), we have shown that this is not the case for haloes with final masses spanning $\sim 10^{11}$–$10^{15}\, h^{-1}\,\text{M}_\odot$, with spin flips, in fact, occurring often without major mergers.

We find that 39 per cent of major mergers coincide with spin flips of 45° or more. Minor mergers or accretion events are very unlikely to coincide with such flips: just 2 per cent of non-major merger events do so. However, the shape of the joint distribution of fractional mass change, $\Delta\mu$, and spin orientation change, $\cos\theta$, is

such that large spin flips are very likely to coincide with non-major-merger events; 76 per cent of spin flips do so.

Changes in spin direction correlate poorly with changes in specific angular momentum magnitude. Spin flips coincide with a broad range of changes in specific angular momentum, albeit with a slight preference for an increase with large flips.

If we consider only those haloes that survive to $z = 0$, then we find that the joint distribution of $\Delta\mu$ and $\cos\theta$ is noticeably narrower in $\Delta\mu$: haloes that are doomed to merge into another halo before $z = 0$ have many more mass-loss events ($\Delta\mu < 0$). This is probably a feature of the merger trees we are using, with haloes losing mass before the time step at which they cease to be recognized as an
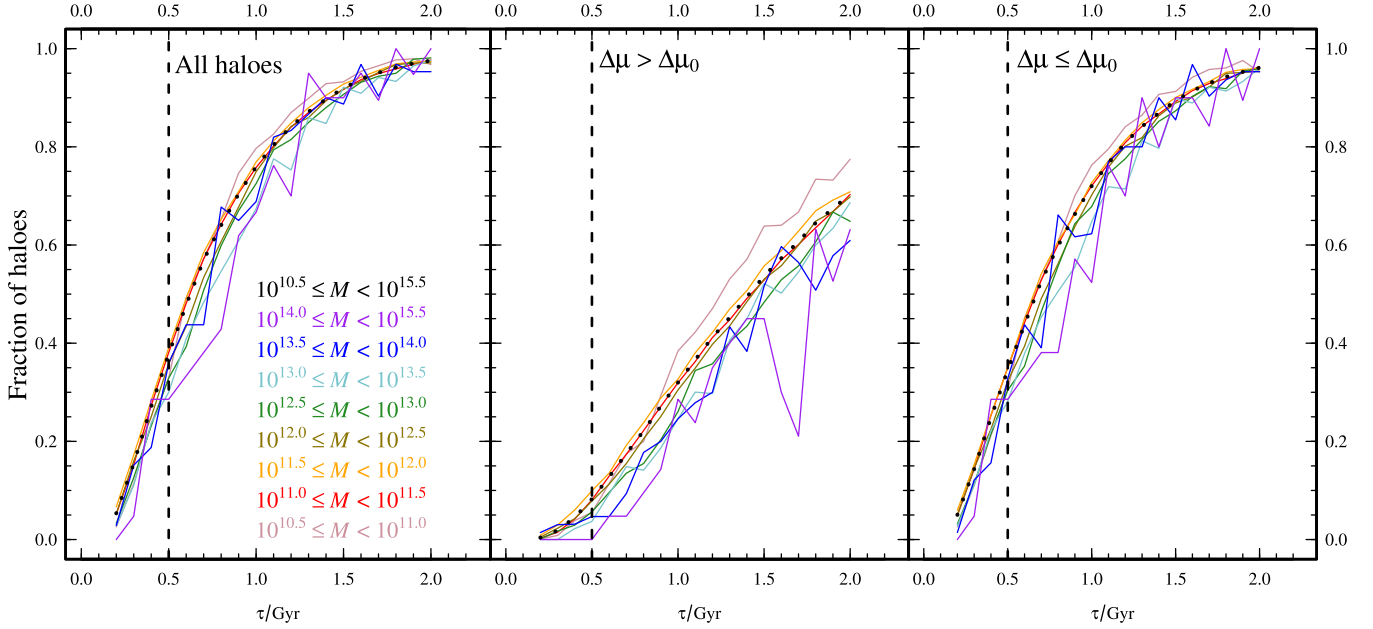
Figure 21. Left: fraction of all halo evolutionary tracks that have at least one spin flip of duration τ and amplitude $\geq 45°$. The middle- and right-hand panels also require that the flip does or does not coincide with a major merger (as in Fig. 19). The haloes are divided into bins, according to their final time mass, colour coded as shown (the masses in the legend are in $h^{-1} M_\odot$). An additional dotted heavy black line shows the results over the whole mass range (this is the same as the 45° line in Fig. 19). Note that the content of the lowest mass bin is affected by our particle-number limit for halo selection: $1000 m_p \approx 10^{10.98} h^{-1} M_\odot$, and the bin upper limit of $10^{11} h^{-1} M_\odot$ corresponds to about 1050 particles. The time-scale used in the rest of the paper, $\tau = 0.5$ Gyr, is marked with a dashed line.
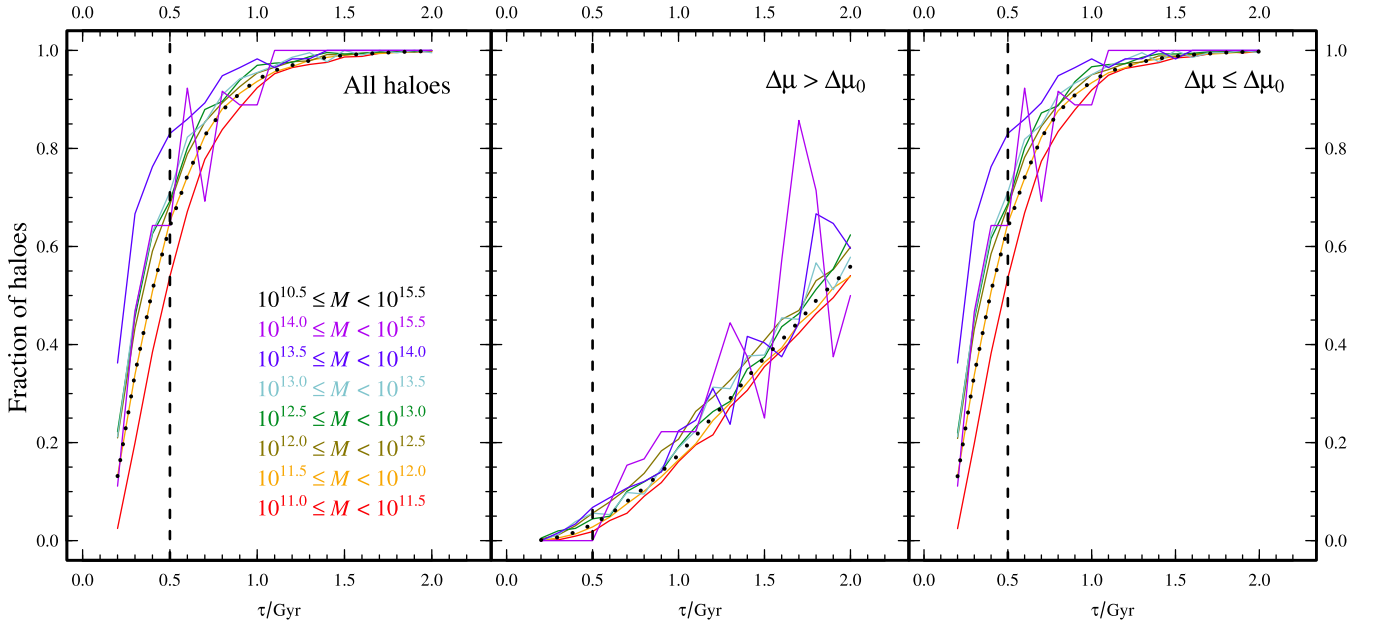

Figure 22. As Fig. 21, but considering flips in the inner halo spin (left), which do (middle) or do not (right) coincide with major mergers. The bins in total-halo final time mass are colour coded as shown (the masses in the legend are in $h^{-1} M_\odot$), with an additional heavy black-dotted line showing the results over the whole mass range (as in Fig. 20).

independent halo. For those haloes that do survive to $z = 0$, we find that less than 1 per cent of minor mergers coincide with large spin flips, but over 95 per cent of large flips coincide with minor mergers.

Since changes in the inner regions of a halo are more likely to have a strong impact on the evolution of the central galaxy, we have also investigated the relationship between flips in the inner halo spin and mergers in the halo as a whole. In this case, we find that there is

a general increase in the probability of a spin flip. In particular, over 95 per cent of large inner flips coincide with minor mergers (over 99 per cent for the haloes that survive to $z = 0$), and 6.3 per cent of minor mergers coincide with a large inner flip.

Many of those large flips that coincide with minor mergers do in fact have a major merger associated with them – but at a slightly earlier or later time step. We have investigated the number of large
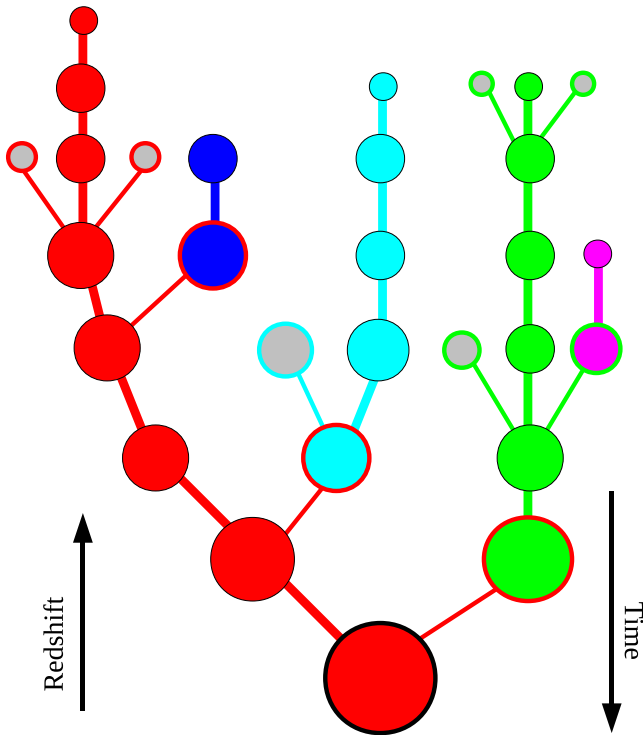
Figure 23. Schematic of a single merger tree, showing immediate progenitors of evolutionary tracks (cf. Fig. 1). The circles represent haloes in the tree at different time steps. Each evolutionary track is given an individual colour (although 'tracks' that only exist for a single time step are all coloured grey). Haloes at the endpoint of their tracks have a heavy outline. When a halo is an immediate progenitor of a halo from a different track, it has that track's colour as an outline.

As in Paper I, we have also considered the likelihood of a large spin flip occurring over the lifetime of a halo, in addition to the distribution of flip events. We find that 37.5 per cent of haloes undergo flips of at least 45° over a time-scale of 0.5 Gyr (64.1 per cent for inner halo flips). Furthermore, despite the broad range of final masses for the haloes we consider ($\sim 10^{11}$–10^{15}), there is little sign of any significant trend in these results with halo mass.

Finally, we have tested how well-conserved halo properties are when going from the set of immediate progenitors at one time step to the single resulting halo at the next time step. Halo models usually assume that halo mass is conserved during mergers (i.e. that the sum of masses of the progenitors equals the mass of the resulting halo), and we find that this is a reasonably good approximation. One might also imagine that the resultant halo's angular momentum is equal to the (vector) sum of those of its immediate progenitors. However, we do *not* find this to be the case. Although 40 per cent of events do have no orientation change between the net spin of progenitors and the final halo spin, the distribution in this orientation change becomes uniform for changes greater than about 45° – i.e. all post-merger orientations greater than 45° are equally probable.

Our findings have consequences for the use of simple halo models, both in theoretical studies and when interpreting observations. Care must be taken when making modelling assumptions related to angular momentum in various contexts. These include the relationship between angular momentum and galaxy morphology; the orientation and persistence of the orientation of haloes with respect to galaxies, and with respect to larger scale structures; and studies that relate dynamical disturbance solely to galaxy mergers.

The present study has not addressed the cause of the non-major merger spin flips that we have observed (although they are presumably related to flybys of satellite haloes, or similar phenomena), and it would be interesting to relate them to properties of the immediate environment of the halo in question. Although we have treated mergers (and for the most part, spin flips) as discrete instantaneous events (albeit with a given time-scale τ), with higher time resolution one would hope to be able to resolve the merger or flip process itself and be able to measure their time-scales directly.

While our choice of algorithms for merger tree, halo definition and selection will have quantitatively affected our results, qualitatively speaking the work presented here can be seen as a warning against using oversimplified halo models of structure and galaxy

flip events that have a major merger within a given time window Δt, and while major mergers can occur before or after large flips, there is a tendency for major mergers to precede the flip. However, even allowing for these inexact coincidences of major mergers and flips, most large flips nevertheless are *never* associated with a major merger, even when Δt is extended to several gigayears.
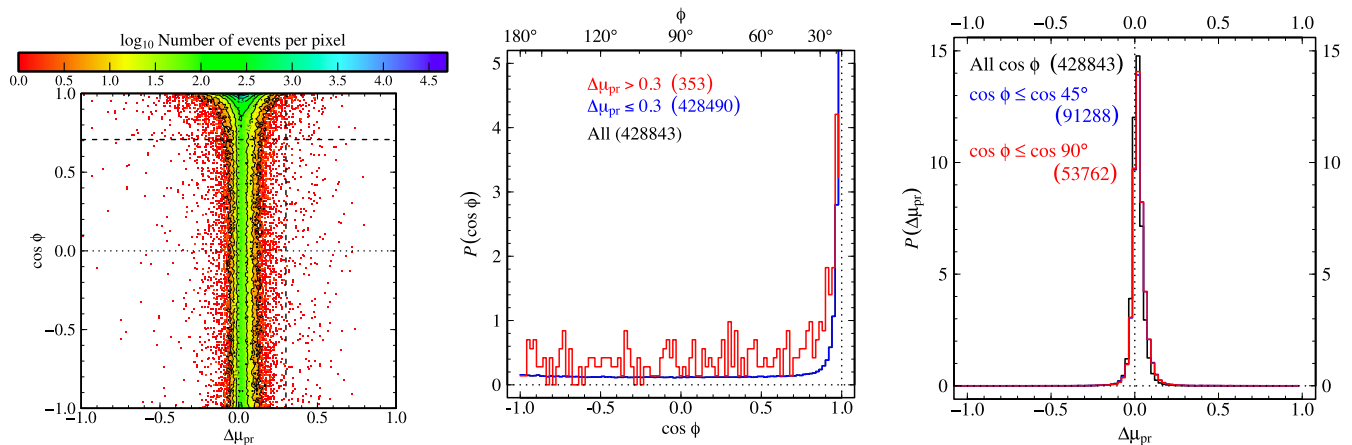
Figure 24. Left: joint distribution of the fractional mass change and spin orientation change between haloes at a given time step and their progenitors at the immediately preceding time step. Middle: histogram showing the distribution across $\cos\phi$, for all events (black), and those when there is a large additional change in mass (red), and when there is not (blue). Right: histogram showing the cross-section through the joint distribution as a function of $\Delta\mu_{pr}$, for all events (black), and events when the total spin changes by at least 45° (blue) and 90° (red).

formation. Haloes can clearly be disturbed by processes related to, but separate from, simply their mass accretion history. Incorporating additional halo properties such as spin direction in models of galaxy formation – perhaps by tracking spin vectors in addition to halo mass – can prove a useful approach to improving their ability to match the observed Universe.

Due to the difficulties in robustly resolving spin changes in simulations (which motivated our series of selection criteria), Padilla et al. (2014) took a statistical approach when implementing spin direction changes in their semi-analytic model, rather than tracking halo spin vectors directly. Further studies of the statistics of spin flips should be carried out in simulations that resolve the dynamics of structures on different scales (at higher resolution and at larger scales), to improve and constrain the implementation of spin flips in semi-analytic galaxy formation models.

REFERENCES

Agustsson I., Brainerd T. G., 2010, ApJ, 709, 1321
Allgood B., Flores R. A., Primack J. R., Kravtsov A. V., Wechsler R. H., Faltenbacher A., Bullock J. S., 2006, MNRAS, 367, 1781
Aumer M., White S. D. M., 2013, MNRAS, 428, 1055
Avila S. et al., 2014, MNRAS, 441, 3488
Avila-Reese V., Colín P., Gottlöber S., Firmani C., Maulbetsch C., 2005, ApJ, 634, 51
Bailin J., Steinmetz M., 2005, ApJ, 627, 647
Barnes J. E., 1988, ApJ, 331, 699
Barnes J. E., 1992, ApJ, 393, 484
Barnes J. E., Hernquist L., 1996, ApJ, 471, 115
Baugh C. M., 2006, Rep. Prog. Phys., 69, 3101
Benson A. J., 2010, Phys. Rep., 495, 33
Benson A. J., Cole S., Frenk C. S., Baugh C. M., Lacey C. G., 2000, MNRAS, 311, 793
Berlind A. A., Weinberg D. H., 2002, ApJ, 575, 587
Bett P. E., 2010, in Debattista V. P., Popescu C. C., eds, AIP Conf. Ser. Vol. 1240, Hunting for the Dark: The Hidden Side of Galaxy Formation. Am. Inst. Phys., New York, p. 403
Bett P. E., Frenk C. S., 2012, MNRAS, 420, 3324 (Paper I)
Bett P., Eke V., Frenk C. S., Jenkins A., Helly J., Navarro J., 2007, MNRAS, 376, 215
Bett P., Eke V., Frenk C. S., Jenkins A., Okamoto T., 2010, MNRAS, 404, 1137
Book L. G., Brooks A., Peter A. H. G., Benson A. J., Governato F., 2011, MNRAS, 411, 1963
Bournaud F., Jog C. J., Combes F., 2005, A&A, 437, 69
Bower R. G., Benson A. J., Malbon R., Helly J. C., Frenk C. S., Baugh C. M., Cole S., Lacey C. G., 2006, MNRAS, 370, 645
Boylan-Kolchin M., Springel V., White S. D. M., Jenkins A., Lemson G., 2009, MNRAS, 398, 1150
Brunino R., Trujillo I., Pearce F. R., Thomas P. A., 2007, MNRAS, 375, 184
Bryan G. L., Norman M. L., 1998, ApJ, 495, 80
Bullock J. S., Dekel A., Kolatt T. S., Kravtsov A. V., Klypin A. A., Porciani C., Primack J. R., 2001, ApJ, 555, 240
Catelan P., Theuns T., 1996a, MNRAS, 282, 436
Catelan P., Theuns T., 1996b, MNRAS, 282, 455
Chen D. N., Jing Y. P., Yoshikawa K., 2003, ApJ, 597, 35
Codis S., Pichon C., Devriendt J., Slyz A., Pogosyan D., Dubois Y., Sousbie T., 2012, MNRAS, 427, 3320
Codis S., Pichon C., Pogosyan D., 2015, MNRAS, 452, 3369
Cox T. J., Dutta S. N., Di Matteo T., Hernquist L., Hopkins P. F., Robertson B., Springel V., 2006, ApJ, 650, 791
Cox T. J., Jonsson P., Somerville R. S., Primack J. R., Dekel A., 2008, MNRAS, 384, 386
Croft R. A. C., Di Matteo T., Springel V., Hernquist L., 2009, MNRAS, 400, 43
Cuesta A. J., Betancort-Rijo J. E., Gottlöber S., Patiri S. G., Yepes G., Prada F., 2008, MNRAS, 385, 867
Davis M., Efstathiou G., Frenk C. S., White S. D. M., 1985, ApJ, 292, 371
De Lucia G., Blaizot J., 2007, MNRAS, 375, 2
Deason A. J. et al., 2011, MNRAS, 415, 2607
Doroshkevich A. G., 1970a, Astrophysics, 6, 320
Doroshkevich A. G., 1970b, Astrofizika, 6, 581
Dubois Y. et al., 2014, MNRAS, 444, 1453
Eke V. R., Cole S., Frenk C. S., 1996, MNRAS, 282, 263
Fakhouri O., Ma C., 2008, MNRAS, 386, 577
Fakhouri O., Ma C., 2009, MNRAS, 394, 1825
Fall S. M., Efstathiou G., 1980, MNRAS, 193, 189
Gao L., Navarro J. F., Cole S., Frenk C. S., White S. D. M., Springel V., Jenkins A., Neto A. F., 2008, MNRAS, 387, 536
Genel S., Genzel R., Bouché N., Naab T., Sternberg A., 2009, ApJ, 701, 2002
Gustafsson M., Fairbairn M., Sommer-Larsen J., 2006, Phys. Rev. D, 74, 123522
Hahn O., Porciani C., Carollo C. M., Dekel A., 2007a, MNRAS, 375, 489
Hahn O., Carollo C. M., Porciani C., Dekel A., 2007b, MNRAS, 381, 41
Hahn O., Teyssier R., Carollo C. M., 2010, MNRAS, 405, 274
Harker G., Cole S., Helly J., Frenk C., Jenkins A., 2006, MNRAS, 367, 1039
Hayashi E., Navarro J. F., Springel V., 2007, MNRAS, 377, 50
Hernquist L., 1992, ApJ, 400, 460
Hernquist L., 1993, ApJ, 409, 548
Hopkins P. F. et al., 2009a, MNRAS, 397, 802
Hopkins P. F., Cox T. J., Younger J. D., Hernquist L., 2009b, ApJ, 691, 1168
Hopkins P. F. et al., 2010, ApJ, 715, 202
Hoyle F., 1951, in Burgers J. M., van de Hulst H. C., eds, Problems of Cosmical Aerodynamics. Central Air Documents Office. Dayton, OH, USA, p. 195
Jiang F., van den Bosch F. C., 2014, MNRAS, 440, 193
Jiang L., Helly J. C., Cole S., Frenk C. S., 2014, MNRAS, 440, 2115
Knebe A., Power C., 2008, ApJ, 678, 621
Knebe A. et al., 2013, MNRAS, 435, 1618
Lemson G., the Virgo Consortium, 2006, preprint (astro-ph/0608019)
Libeskind N. I., Frenk C. S., Cole S., Jenkins A., Helly J. C., 2009, MNRAS, 399, 550
Libeskind N. I., Hoffman Y., Knebe A., Steinmetz M., Gottlöber S., Metuki O., Yepes G., 2012, MNRAS, 421, L137
Łokas E. L., Mamon G. A., 2001, MNRAS, 321, 155

Macciò A. V., Dutton A. A., van den Bosch F. C., Moore B., Potter D., Stadel J., 2007, MNRAS, 378, 55

Macciò A. V., Dutton A. A., van den Bosch F. C., 2008, MNRAS, 391, 1940

Maller A. H., Katz N., Kereš D., Davé R., Weinberg D. H., 2006, ApJ, 647, 763

Mo H. J., Mao S., White S. D. M., 1998, MNRAS, 295, 319

Moster B. P., Macciò A. V., Somerville R. S., Johansson P. H., Naab T., 2010, MNRAS, 403, 1009

Muñoz-Cuartas J. C., Macciò A. V., Gottlöber S., Dutton A. A., 2011, MNRAS, 411, 584

Naab T., Burkert A., 2003, ApJ, 597, 893

Navarro J. F., Frenk C. S., White S. D. M., 1996, ApJ, 462, 563

Navarro J. F., Frenk C. S., White S. D. M., 1997, ApJ, 490, 493

Neistein E., Macciò A. V., Dekel A., 2010, MNRAS, 403, 984

Neto A. F. et al., 2007, MNRAS, 381, 1450

Okamoto T., Eke V. R., Frenk C. S., Jenkins A., 2005, MNRAS, 363, 1299

Padilla N. D., Salazar-Albornoz S., Contreras S., Cora S. A., Ruiz A. N., 2014, MNRAS, 443, 2801

Paz D. J., Stasyszyn F., Padilla N. D., 2008, MNRAS, 389, 1127

Peebles P. J. E., 1969, ApJ, 155, 393

Porciani C., Dekel A., Hoffman Y., 2002, MNRAS, 332, 325

Romano-Díaz E., Shlosman I., Heller C., Hoffman Y., 2009, ApJ, 702, 1250

Scannapieco C., White S. D. M., Springel V., Tissera P. B., 2009, MNRAS, 396, 696

Schäfer B. M., 2009, Int. J. Mod. Phys. D, 18, 173

Shaw L. D., Weller J., Ostriker J. P., Bode P., 2006, ApJ, 646, 815

Springel V., White S. D. M., Tormen G., Kauffmann G., 2001, MNRAS, 328, 726

Springel V. et al., 2005, Nature, 435, 629

Srisawat C. et al., 2013, MNRAS, 436, 150

Stewart K. R., Bullock J. S., Wechsler R. H., Maller A. H., Zentner A. R., 2008, ApJ, 683, 597

Stewart K. R., Bullock J. S., Wechsler R. H., Maller A. H., 2009, ApJ, 702, 307

Sugerman B., Summers F. J., Kamionkowski M., 2000, MNRAS, 311, 762

Toomre A., 1977, in Tinsley B. M., Larson R. B., eds, Evolution of Galaxies and Stellar Populations. Yale Univ. Observatory, New Haven, p. 401

Toomre A., Toomre J., 1972, ApJ, 178, 623

Tweed D., Devriendt J., Blaizot J., Colombi S., Slyz A., 2009, A&A, 506, 647

van den Bosch F. C., Abel T., Croft R. A. C., Hernquist L., White S. D. M., 2002, ApJ, 576, 21

van den Bosch F. C., Abel T., Hernquist L., 2003, MNRAS, 346, 177

Warren M. S., Quinn P. J., Salmon J. K., Zurek W. H., 1992, ApJ, 399, 405

Wechsler R. H., Bullock J. S., Primack J. R., Kravtsov A. V., Dekel A., 2002, ApJ, 568, 52

Welker C., Devriendt J., Dubois Y., Pichon C., Peirani S., 2014, MNRAS, 445, L46

Welker C., Dubois Y., Devriendt J., Pichon C., Kaviraj S., Peirani S., 2015, preprint (arXiv:1502.05053)

White S. D. M., 1984, ApJ, 286, 38

White S. D. M., Frenk C. S., 1991, ApJ, 379, 52

White S. D. M., Rees M. J., 1978, MNRAS, 183, 341

Zavala J., Okamoto T., Frenk C. S., 2008, MNRAS, 387, 364

APPENDIX A: CHOICE OF HALO EVENT TIME-SCALE

We wish to find an appropriate characteristic time-scale of haloes to use for calculating changes in halo properties. While we expect such a time-scale to depend on cosmology, redshift, and halo mass, we aim to find a *single* value that we can use throughout our analysis. We will compare our results at different time-scales to demonstrate the degree to which they depend on this choice of time-scale.

In general, we can write a time-scale as $\tau = \ell/v$. We take the characteristic length ℓ to be some multiple of a characteristic halo radius yr, where for example $y = 2$, π, 2π, etc, making ℓ the diameter, circumference, etc. We take the characteristic velocity, v, to be the circular velocity of a test particle at r orbiting under gravity, $v = \sqrt{GM(<r)/r}$. The time-scale is therefore given by

$$\tau = y\sqrt{\frac{r^3}{GM(<r)}}. \tag{A1}$$

If we model a halo as the mass within a particular spherical boundary set by an overdensity criterion, and we take $r = R_{\rm vir}$, then $M(<r) \equiv M_{\rm vir} = \frac{4}{3}\pi R_{\rm vir}^3 \Delta_{\rm c}(z)\rho_{\rm crit}(z)$. Defining for convenience $\chi(z) = \Omega_{\rm M0}a^{-3} + \Omega_{\Lambda 0}$, we can write $\rho_{\rm crit} = \chi(z)\rho_{\rm crit,0} = \chi(z)3H_0^2/8\pi G$, giving

$$\tau(z) = y\sqrt{\frac{3}{4\pi G}\frac{8\pi G}{3H_0^2}\frac{1}{\chi(z)\Delta_{\rm c}(z)}} \equiv \frac{y}{H_0}\sqrt{\frac{2}{\chi(z)\Delta_{\rm c}(z)}}. \tag{A2}$$

Since our definition of $R_{\rm vir}$ depends only on cosmology and time, so also does τ – losing any dependence on halo properties, making it a cosmological time-scale rather than a halo time-scale. In fact, since the overdensity criterion, $\Delta_{\rm c}(z)$, originates in the spherical collapse model of halo formation, this time-scale is that of the haloes that are forming at redshift z, rather than of the spectrum of extant haloes at that redshift.

An alternative is to take the characteristic radius somewhere within $R_{\rm vir}$, thus, incorporating the halo density profile and retaining some dependence on halo scale and history. If we take the characteristic radius as that enclosing some fraction of the halo mass, i.e. $f_{\rm M} = M(<R_f)/M_{\rm vir}$, and $r = R_f$, then equation (A1) becomes

$$\tau = y\sqrt{\frac{R_f^3}{Gf_{\rm M}M_{\rm vir}}} \tag{A3}$$

$$= y\sqrt{\frac{3}{4\pi G}\frac{8\pi G}{3H_0^2}\frac{R_f^3}{f_{\rm M}R_{\rm vir}^3}\frac{1}{\chi(z)\Delta_{\rm c}(z)}} \tag{A4}$$

$$= \frac{y}{H_0}\sqrt{\frac{R_f^3}{f_{\rm M}R_{\rm vir}^3}\frac{2}{\chi(z)\Delta_{\rm c}(z)}}. \tag{A5}$$

We now assume an NFW density profile (Navarro, Frenk & White 1996, 1997),

$$\rho(r) = \frac{\rho_{\rm s}}{\frac{r}{r_{\rm s}}\left(1+\frac{r}{r_{\rm s}}\right)^2}, \tag{A6}$$

where the halo concentration is related to the scale radius through $c = R_{\rm vir}/r_{\rm s}$, and the characteristic density is

$$\rho_{\rm s} = \frac{\Delta_{\rm c}\rho_{\rm crit}}{3}\frac{c^3}{\left(\ln(1+c) - \frac{c}{1+c}\right)}. \tag{A7}$$

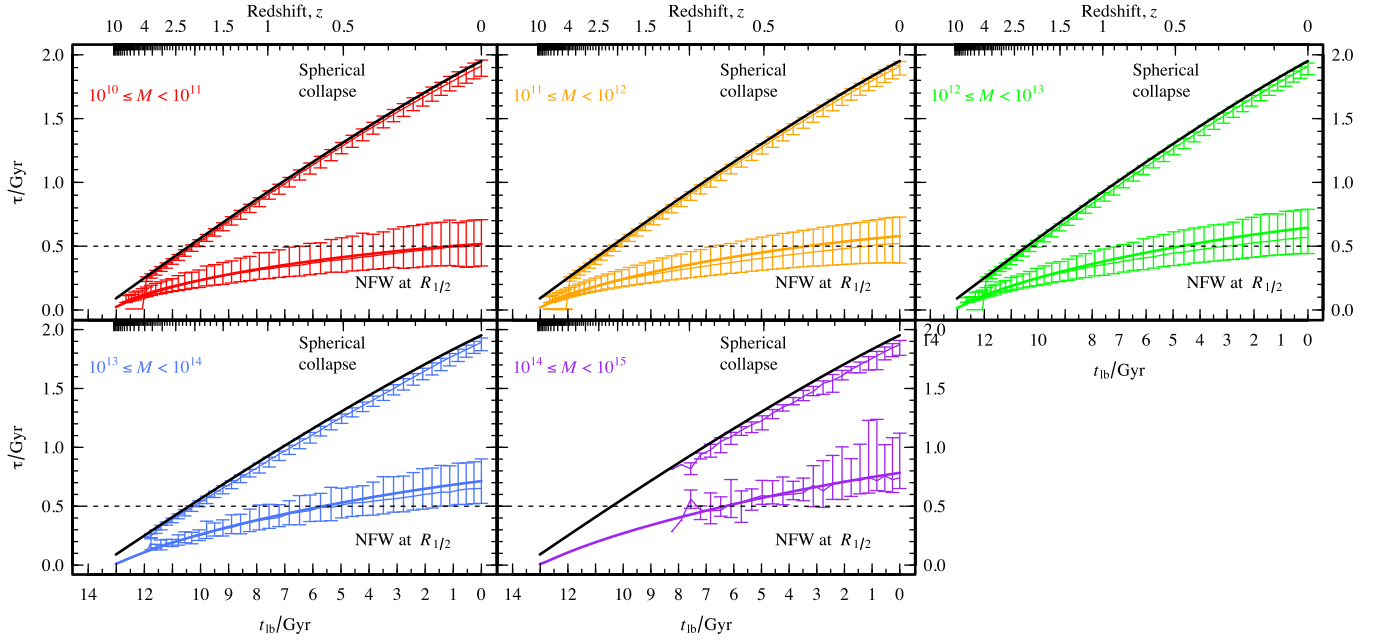The cumulative mass is $M(<R) = 4\pi\int_0^R \rho(r)r\,{\rm d}r$, so here

$$M(<R) = 4\pi\rho_{\rm s}\int_0^R \frac{r^2}{\frac{r}{r_{\rm s}}\left(1+\frac{r}{r_{\rm s}}\right)^2}{\rm d}r. \tag{A8}$$

If we define $x = r/R_{\rm vir}$ so that $cx = r/r_{\rm s}$, we get

$$M(<R_{\rm vir}) = 4\pi\rho_{\rm s}\frac{R_{\rm vir}^3}{c^3}\left(\ln(1+cx) - \frac{cx}{1+cx}\right) \tag{A9}$$

$$= \frac{4}{3}\pi R_{\rm vir}^3\Delta_{\rm c}(z)\rho_{\rm crit}(z)\left(\frac{\ln(1+cx) - \frac{cx}{1+cx}}{\ln(1+c) - \frac{c}{1+c}}\right). \tag{A10}$$

Figure A1. Different halo time-scales as a function of look back time, t_{lb}, with each panel showing haloes of different masses at each snapshot. The lines labelled 'Spherical collapse' use the halo-independent time-scale: the analytic result from equation (A2) (solid black line) is compared to the medians and 10th/90th percentiles (points and error bars) from the distribution of measured time-scales from the haloes at each snapshot, using equation (A1) with $r = R_{vir}$. The data labelled 'NFW at $R_{1/2}$' shows the time-scale at the half-mass radius: the solid lines are from equation (A5) with $f_M = 1/2$, assuming an NFW profile and using the fitting formulae (see text; Muñoz-Cuartas et al. 2011; Łokas & Mamon 2001). The points again show the medians and percentiles of the measured time-scale (equation (A1) with $r = R_{1/2}$) from haloes in mass bins at each snapshot.

The radius fraction, x, for a given concentration can then be found by solving

$$\ln(1 + cx) - \frac{cx}{1 + cx} = f_M \left(\ln(1 + c) - \frac{c}{1 + c} \right). \qquad (A11)$$

In the case of $f_M = 1/2$, Łokas & Mamon (2001) provided a fitting formula for $x(c)$ and thus the half-mass radius, $R_{1/2}$.

To link this back to the halo mass and radius, we need a concentration–mass relation for all redshifts; fitting formulae for such a relation are provided, for example, in Muñoz-Cuartas et al. (2011). So, for a given halo mass and desired fraction f_M, at a given redshift, we can find a concentration and thus $x = R_f/R_{vir}$, and finally τ.

Fig. A1 shows the time-scales from the above equations (A2) and (A5) (in the latter taking $f_M = 1/2$ so $R_f = R_{1/2}$), along with the time-scales *measured* from haloes at each time step, using $\tau_{meas} = \sqrt{R_{vir}^3/(GM_h)}$ and $\tau_{1/2,meas} = \sqrt{2R_{1/2}^3/(GM_h)}$. (Haloes are selected in this case only if they have at least 1000 particles.) The results from the haloes themselves match the analytic results very

well in all cases. Given the mass distribution of our haloes over the time period of interest, we opt to use a single value of $\tau = 0.5\,\text{Gyr}$ for analysing halo property changes. Using a single value makes for more straightforward comparisons and analysis as haloes grow and evolve, and the results presented above show that this is a reasonable approximation for our haloes.

We expect the choice of time-scale to affect our results quantitatively, but not qualitatively. While some of our results are already shown as a function of measurement time-scale (see section 3.4), we show, here, how the event distribution varies with the choice of τ. Fig. A2 compares the event distribution from Fig. 2 (i.e. using $\tau = 0.5\,\text{Gyr}$), with that obtained when values of $\tau = 0.3$ and 1.0 Gyr are used, and when just the (variable) intersnapshot time step is used. These show that, in practice, there is very little difference between the universal time-scale we choose and just looking at property differences between snapshots. In contrast, using a longer time-scale produces a broader distribution, with more events spread away from the 'no change' point, and using a shorter time-scale produces a tighter distribution. It seems that spin orientation change $\cos\theta$ is affected more than the fractional mass change $\Delta\mu$.
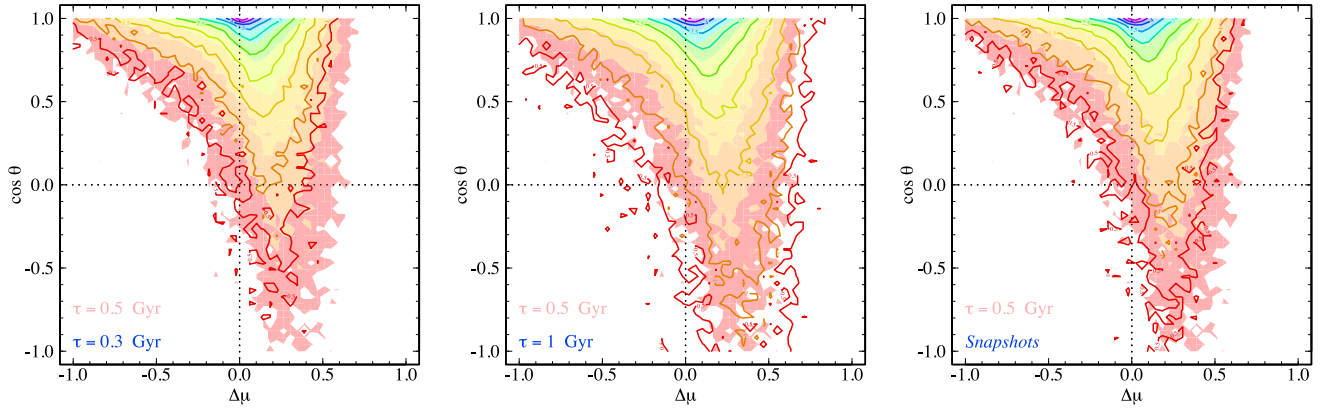
Figure A2. Contour plots of event distributions following that of Fig. 2. Those results are shown as filled contours. The outline contours show the results of varying the choice of τ, with the left-hand panel using a shorter time-scale, the middle panel using a longer time-scale. The right-hand panel uses the time difference between the simulation snapshots directly, without interpolation (i.e. a variable time-scale between 0.4 and 0.1 Gyr.). The same selection criteria as in Fig. 2 are used in all cases.

This paper has been typeset from a TEX/LATEX file prepared by the author.